Ref. Ares(2021)2952245 - 04/05/2021

PROJECT DELIVERABLE REPORT

Project Title:
Advanced personalised, multi-scale computer models preventing osteoarthritis
SC1-PM-17-2017 - Personalised computer models and in-silico systems for well-being

Deliverable number	D3.2
Deliverable title	OACTIVE biomechanical simulation and analysis engines
Submission month of deliverable	M41
Issuing partner	CERTH
Contributing partners	LJMU, UPAT, KUL
Dissemination Level (PU/PP/RE/CO):	PU
Project coordinator	University of Nicosia (UNIC)
Tel:	**+357 22 841 528**
Fax:	**+357 22 357481**
Email:	**felekkis.k@unic.ac.cy& giannaki.c@unic.ac.cy**
Project web site address	www.oactive.eu

Revision History

Version	**Date**	**Responsible**	**Description/Remarks/Reason for changes**
1.0		LJMU,CERTH	First Draft
1.1		LJMU,CERTH	Review of First Draft
1.2		LJMU, CERTH, UPAT, KUL	Review of Second Draft

Contents

1 Introduction

Neuromusculoskeletal and finite element pipelines are a key output of the OACTIVE project. Pipelines have been developed to allow the measuring of subject specific biomechanical parameters in the joints of subjects recruited for the OACTIVE project and these form a key input to the neural networking modules developed elsewhere. Deliverable 3.1 described the overall pipelines as well as detailed documentation describing the individual components of this pipeline and how they can be used to produce subject specific knee joint biomechanics. Deliverable 3.2, as presented here, follows on from this and outlines the key outputs from the neuromusculoskeletal and finite element models developed as part of the OACTIVE project.

To start with, a large cohort study is described, where key biomechanical variables from the musculoskeletal pipeline are compared between groups with and without osteoarthritis collected as a part of the OACTIVE project. Following on from this, a series of studies were undertaken to parameterize and investigate the effect of certain variables on key outputs from the finite element pipelines in order to understand more the effect of model complexity on the important outputs. More advanced subject specific finite element models were then constructed for a series of subjects with and without the incidence of knee OA and these are used to identify differences between subjects of differing disease severity. Finally, a series of ongoing studies are described that are aiming to use the technologies and tools developed in WP3 to advance our understanding of both the technologies themselves and how they can be applied to other clinical datasets outside of OACTIVE.

2 Summary of Neuromusculoskeletal Pipelines

2.1 Introduction

This section includes a summary of the methods developed as part of the OACTIVE project to evaluate subject specific joint loading in the OACTIVE subjects. The outputs from these models form the key content of this deliverable, and the methods used to generate these output is described briefly here so that the document can function independently of other deliverables. Much of this information has been included already in D3.1 and that should be consulted if more detailed information than that provided here is required

2.2 Musculoskeletal Modelling Pipeline

3D gait analysis was undertaken on 143 subjects across the three different clinical partners involved in the OACTIVE project. Motion capture data was collected for each patient using standard motion capture techniques. This included the collection of marker based kinematic data as well as kinetic data from force plates. Reflective markers were placed on the subject at predefined positions. The marker set used was an updated version of the conventional gait model (CGM) dataset (CGM2.1), with 28 markers on the lower limbs. The model differs from previous versions of the CGM in that it includes a series of 3 markers on both the femur and shank (LTHAP, LTHI, LTAD; LTIAP, LTIB, LTIAD). For each patient a static trial was captured, as well as functional trials for both the knee and hip for joint centre calculation. Dynamic trials of the subject walking and stepping up and over a step were also collected. Following this, this data was pre-processed using Vicon Nexus 2.1 where marker locations were reconstructed and synced with ground reaction force data. SCORE and SARA algorithms were used to identify the location of subject specific hip joint centres and knee joint axes from functional joint rotation trials. Data was processed and exported using a standard workflow, with gaps in marker trajectories being filled and markers being labelled appropriately. Analog data from force plates was exported as .mot files, with dynamic data from the marker trajectories being exported as .trc files. A custom MATLAB script was used to calculate the knee joint centre of rotation as the intersection of the functional knee joint axis with a plane passing through the hip joint centre, the midpoint of the lateral and medial knee markers and the ankle joint centre. The ankle joint centre was calculated as the midpoint of the lateral and medial ankle markers.

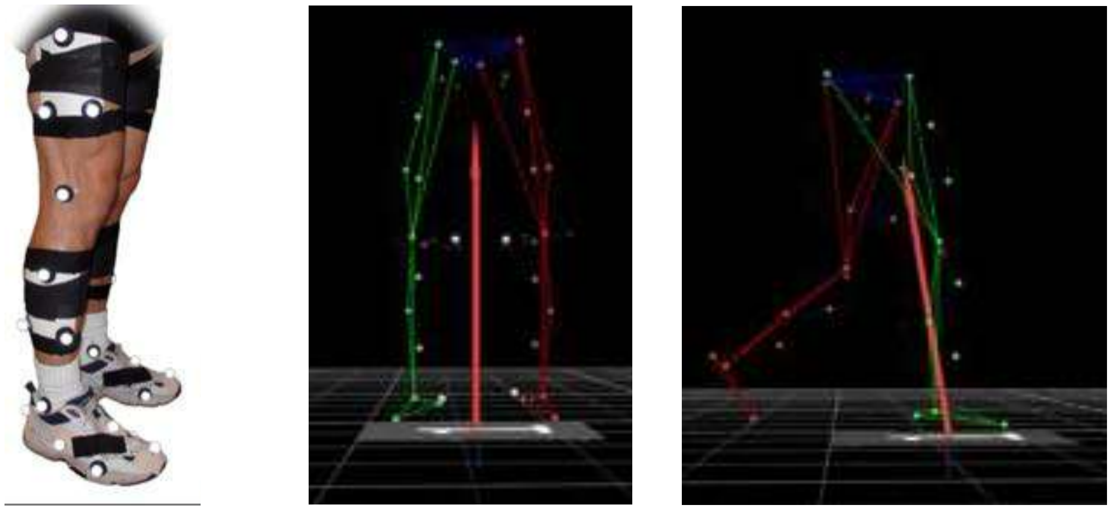

Figure 1 - 3D gait analysis. Left: Example of marker placement on leg of subject. Middle: Reconstructed markers and ground reaction force data for static trial. Right: Reconstruction of marker data and ground reaction forces for gait trial

Once the data had been pre-processed, a generic model was scaled in OpenSim to match as best as possible the anatomy of the subject under consideration. The generic model consists of 12 segments, a torso, pelvis, left and right thigh, shank, talus, calcaneus and toes. Marker data from a static trial was used to carry out the scaling along with the locations of the functional joint centres. OpenSim was then used to perform inverse kinematics and inverse dynamics using the scaled model to generate joint kinematics and moments. Static optimization was then used to derive musculotendon and joint contact forces in OpenSim. Data from processed OpenSim files was collated using custom MATLAB routines. Knee joint kinematics and kinetics were extracted for each trial and normalized in the time domain.

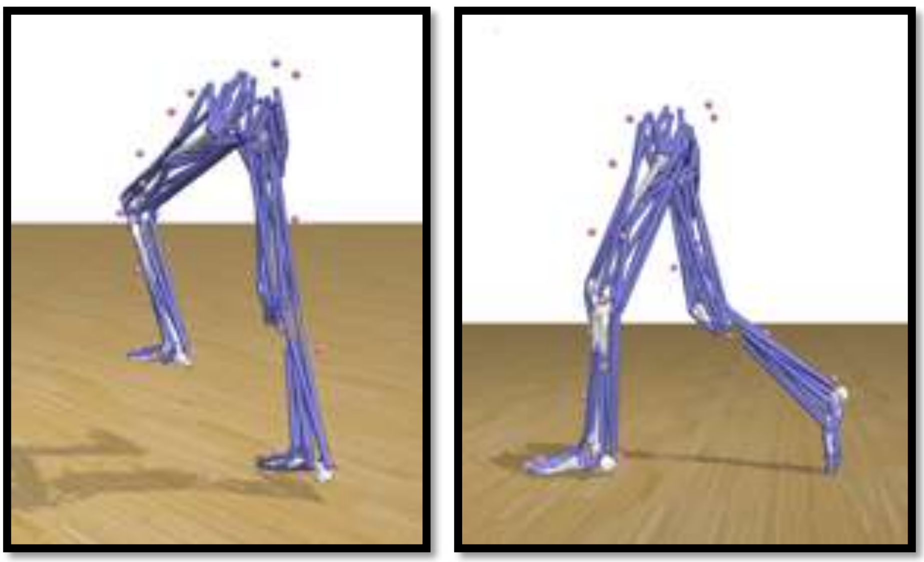

Figure 2 - OpenSim processing showing reconstruction of scaled subject specific model undergoing stepping andwalking

2.3 Finite Element Pipeline

MRI images from the subjects were segmented manually in order to extract the surface geometries of the femur, tibia, tibial cartilage, femoral cartilage and menisci. Each significant part of the anatomical structure (i.e. femur, femoral cartilage etc.) was segmented on their own as it is necessary for the mesh generation and the assignment of material properties later in the process. Following the export of the surface STL files containing the geometry of the relevant anatomy, the files are imported in MeshLab in order to smooth and refine the meshes using a combination of Laplacian and Taubin filters. The smoothed mesh elements are then exported as surface files and imported into FeBio Studio for the construction of the FE model. Material properties are defined and applied to each material as per the table below. The tibial and femoral cartilages are modelled as Mooney-Rivlin type materials, the menisci as fung orthotropic and the tibia and femoral bones modelled as rigid bodies. Contact surfaces are then defined to allow for frictionless motion between the articulating surfaces of the cartilage and with the respective surfaces of the menisci. Two simulation steps are then created, the first to allow for simple pre-loading, where a small load is applied so that the femoral and tibial components can meet. During this phase the tibia is constrained in all six degrees of freedom whilst the femur is allowed to translate vertically. During the second simulation step, the constraints on the femur are relaxed so that it can rotate in both the flexion/extension axis and the adduction/abduction axis whilst still being able to translate vertically. During this step the loading is slowly increased gradually in all three axis until it reaches the peak loading during either the first or second half of the stance phase respectively. The flexion angle is also adjusted gradually so that it reaches the flexion angle experienced by the subject when it is undergoing the respective loading. The joint loading and flexion angles applied are subject specific and are found using the musculokskeletal approaches described earlier. Peak cartilage stresses, strains, deformations, contact areas and contact forces are then extracted manually using FEBio Studio at the end of each simulation from the surfaces of the tibial and femoral cartilage and recorded for further analysis

3 Effect of incident KOA on knee joint biomechanics

3.1 *Introduction*

This section includes a summary of the musculoskeletal models developed as part of the OACTIVE project as well as an investigation into any differences seen between different clinical groups.

3.2 *Methods*

Subject selection and stratification

The subjects were split into three categories based on their measured Kellgren Lawrence (KL) scores. These were healthy (KL=0), mild KOA (KL=1) and moderate KOA (KL=2). Subjects who did not have KL scores recorded were not considered as part of this study. Six subjects from UNIC were excluded from this comparative study as the data collection protocol was slightly different and there was no control group from that centre, making it difficult to determine if merging the data with other centres was appropriate. A summary of the selected groups is found in the table below, with the KL score of the subjects alongside the average age, body mass, gender and BMI of each group.

Group	KL	N	Age (yrs)	Mass (kg)	Height (m)	BMI	Males (%)
Healthy	0	62	43 (16)	74.8 (12.4)	1.69 (0.08)	25.9 (4.03)	45.4
Mild KOA	1	16	39 (24)	78.3 (17.6)	1.69 (0.07)	27.3 (5.53)	56.3
Moderate KOA	2	6	44 (27)	81.0 (8.9)	1.77 (0.09)	25.8 (2.75)	87.5

3.3 Results

Knee Flexion Angles

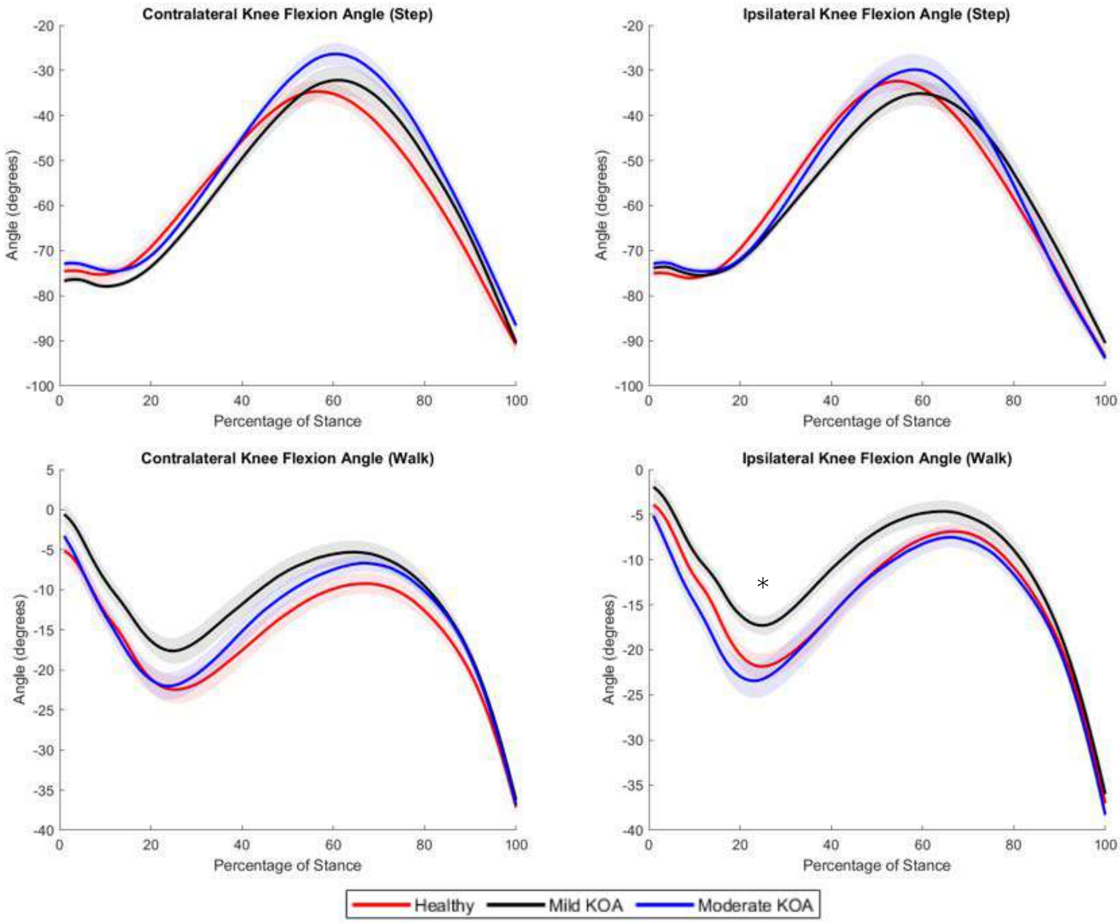

*Figure 3 - Graphs showing knee joint flexion angles during the stance phase for walking and stepping trials in the ipsilateral and contralateral limbs of healthy, mild KOA and moderate KOA subjects. Increased flexion is indicated by more negative joint angles. Solid lines represent the mean joint angles, whilst shaded areas represent the 95% confidence intervals for those means. *Statistically significant differences found (p<0.1) ** Statistically significant differences (p<0.05)*

Knee flexion moments for healthy, mild KOA and moderate KOA subjects undergoing stepping and walking trials are shown in Figure 3. Knee flexion angles followed similar patterns for all three groups for both walking and stepping. During walking, the knee flexes after heel strike, extends during the loading phase of the stance and then flexes again prior to toe off. For stepping this pattern shifts slightly, with the knee starting in a heavily flexed position, extending as the subjects step up onto the step and the flexing again prior to toe-off. When looking at differences between groups there were no significant relationships found for knee flexion angle during stepping trials. During walking trials there was some evidence found that peak flexion during the first half of stance was reduced in the ipsilateral limb of subjects with mild KOA compared to controls ($p<0.1$), whilst subjects with moderate KOA showed no significant differences.

Knee Abduction Angles

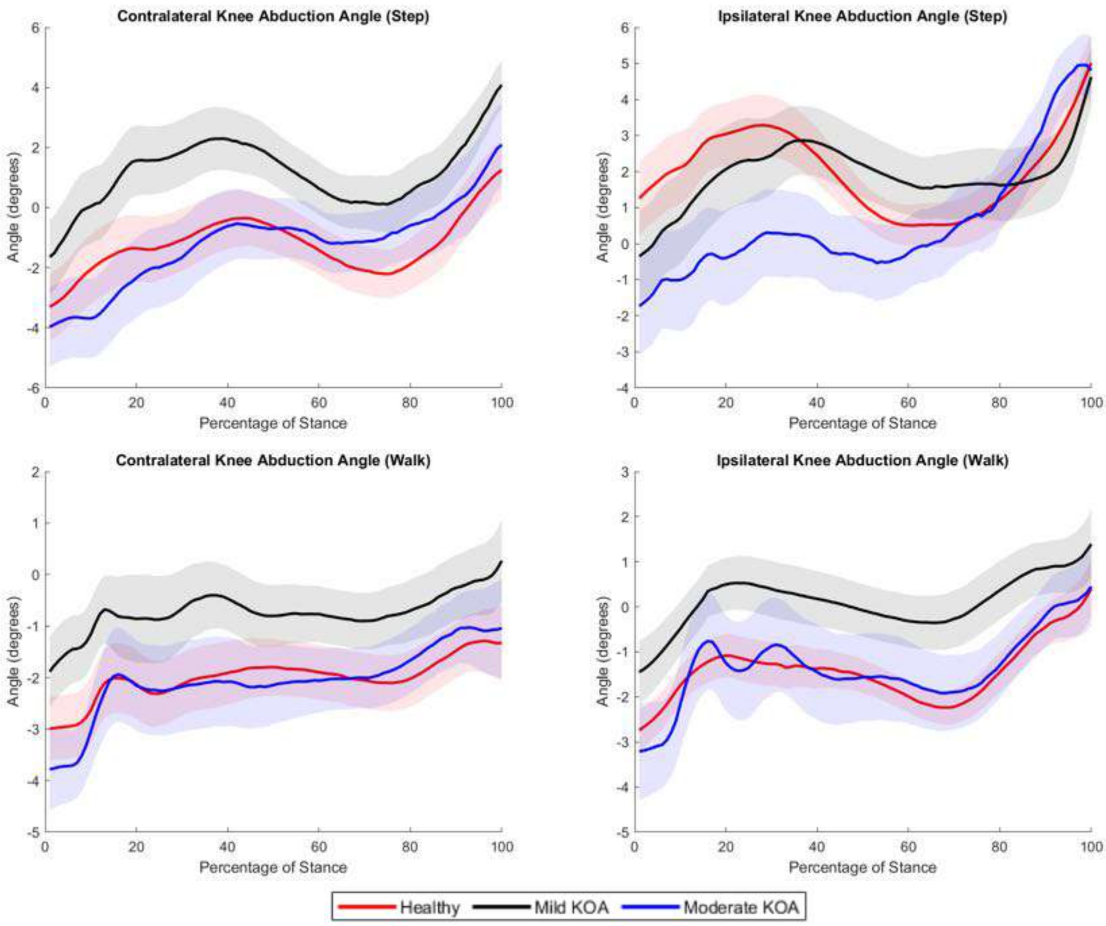

*Figure 4 - Graphs showing knee joint abduction angles during the stance phase for walking and stepping trials in the ipsilateral and contralateral limbs of healthy (n=62), mild KOA (n=16) and moderate KOA subjects (n=6). Increased abduction is indicated by more positive joint angles. Solid lines represent the mean joint angles, whilst shaded areas represent the 95% confidence intervals for those means. *Statistically significant differences found (p<0.1) ** Statistically significant differences (p<0.05)*

Knee abduction angles for healthy, mild KOA and moderate KOA subjects undergoing stepping and walking trials are shown in Figure 4. Knee joint abduction angles also followed similar trends for all subject groups in both stepping and walking trials. The knee abducts slightly following heel strike, adducts during the loading phase and then abducts again prior to toe off. Statistical testing showed that there were no significant differences in peak abduction angles during the first and second half of stance between the three groups. Subjects with mild KOA appear to have slightly elevated knee abduction throughout the stance phase but the large amount of inter subject variation meant it was not possible to determine the veracity of any changes seen visually.

Knee Flexion Moments

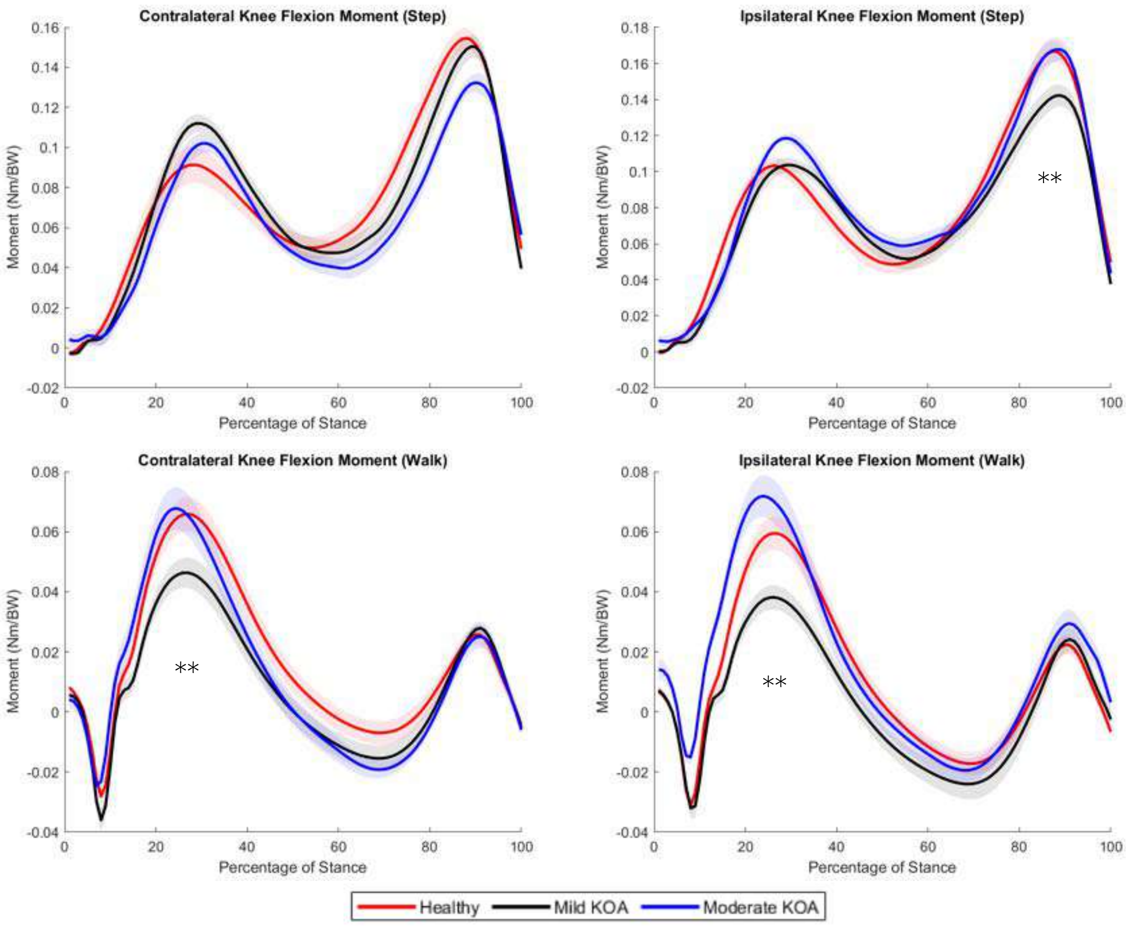

*Figure 5 - Graphs showing knee joint flexion moments during the stance phase for walking and stepping trials in the ipsilateral and contralateral limbs of healthy (n=62), mild KOA (n=16) and moderate KOA (n=6) subjects. Increased flexion moments are indicated by more positive joint angles. Solid lines represent the mean joint moments, whilst shaded areas represent the 95% confidence intervals for those means. *Statistically significant differences found (p<0.1) ** Statistically significant differences (p<0.05)*

Knee flexion moments for healthy, mild KOA and moderate KOA subjects undergoing stepping and walking trials are shown in Figure 5. During walking, net extension moments shortly after heel strike were followed by a classic double peak curve, with a large peak flexion moment during the first half of stance and a smaller peak flexion moment during the second half of stance. Flexion moments for subjects undergoing stepping movements are seen to be net flexor throughout, with a smaller peak during the first half of stance followed by a second, larger peak during the second half. Peak flexion and extension moments during the first and second half of stance were extracted and tested for statistical significance. It was found that the second peak flexion moment in the ipsilateral knee was significantly smaller for mild KOA subjects than healthy subjects during stepping ($p<0.05$). It was also found that the peak flexion moment during the first half of stance was significantly lower for mild KOA subjects in both the ipsilateral ($p<0.05$) and contralateral ($p<0.05$) knees.

Abduction Moments

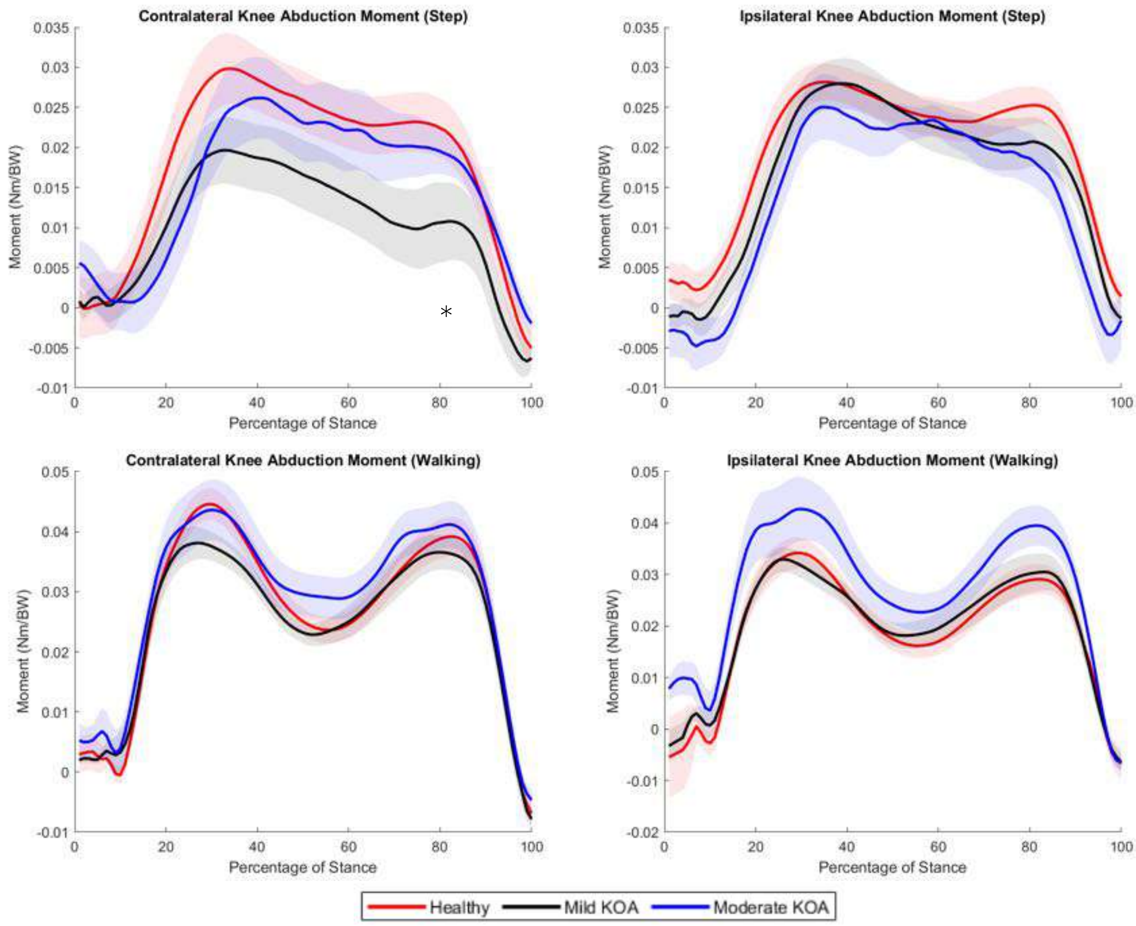

*Figure 6 - Graphs showing knee joint abduction moments during the stance phase for walking and stepping trials in the ipsilateral and contralateral limbs of healthy (n=62), mild KOA (n=16) and moderate KOA (n=6) subjects. Increased abduction moments are indicated by more positive joint angles. Solid lines represent the mean joint moments, whilst shaded areas represent the 95% confidence intervals for those means. *Statistically significant differences found (p<0.1) ** Statistically significant differences (p<0.05)*

Figure 6 shows the knee abduction moment during the stance phase of stepping and walking trials for healthy, mild KOA and moderate KOA subjects. Abduction moments for walking trials followed a double peak curve with almost equal peak abduction moments occurring during the first and second half of stance. Abduction moments for stepping trials were slightly lower on average, and had a less defined double peak shape, with a plateau occurring between the first and second peaks. Peak abduction moments during the first and second half of stance were extracted and tested for statistical significance. The second peak abduction moment in the contralateral knee was seen to be somewhat lower for mild KOA subjects than healthy ones ($p<0.1$), but no other significant changes were seen during stepping. No significant differences were found between any of the subjects during walking trials. Abduction moments in the ipsilateral knee appear to be slightly higher throughout the stance phase for subjects with moderate KOA, but this did not reach the level of significance at any time point.

Joint Contact Forces

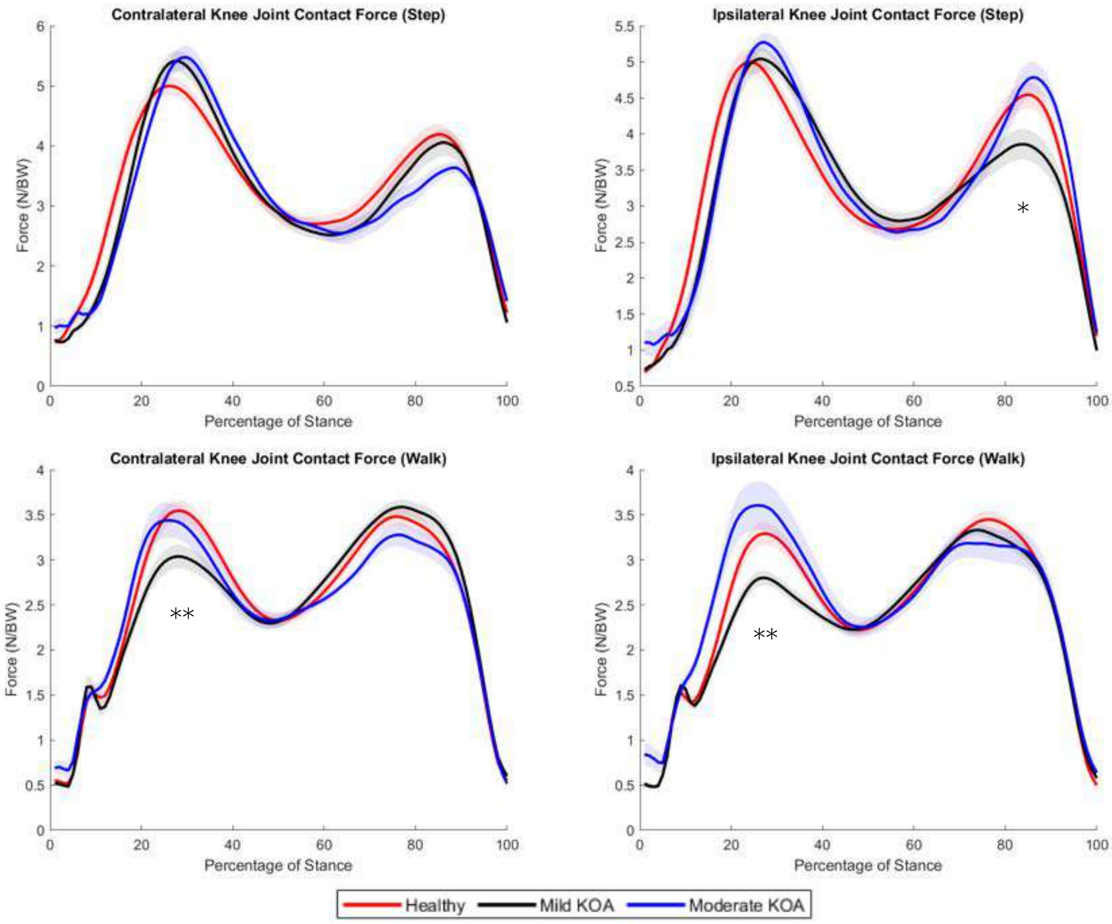

*Figure 7 - Graphs showing compressive knee joint contact forces during the stance phase for walking and stepping trials in the ipsilateral and contralateral limbs of healthy (n=62), mild KOA (n=16) and moderate KOA subjects (n=6). Increased forces are indicated by more positive joint angles. Solid lines represent the mean joint forces, whilst shaded areas represent the 95% confidence intervals for those means. *Statistically significant differences found (p<0.1) ** Statistically significant differences (p<0.05)*

Joint contact forces at the knee are shown in Figure 7 for the ipsilateral and contralateral knees of healthy, mild KOA and moderate KOA subjects undergoing stepping and walking trials. Contact forces follow the traditional double peak pattern for stepping and walking trials with peaks occurring in the first and second half of stance. These peaks were extracted, and statistical tests were used to test for differences between the three stratified groups. Subjects with mild KOA had somewhat reduced contact forces during the second half of stance in the ipsilateral limb during stepping ($p<0.1$) compared to control subjects. They also have significantly lower forces in the first half of stance during gait in both legs ($p<0.05$). No differences were found between the moderate KOA subjects and either the healthy subjects or those with mild KOA.

Summary Table

Table 1 and Table 2 below show a summary of the kinematic and kinetic variables extracted as part of this analysis for walking and stepping trials respectively. Significant differences found between osteoarthritic and healthy groups are shown alongside the level of that significance.

*Table 1 - Summary of biomechanical data for OACTIVE subjects walking showing ipsilateral and contralateral knee joint angles, moments and forces during the first and second half of stance for healthy, mild KOA and moderate KOA subjects. *significantly different to healthy group (p<0.1) ** significantly different to healthy group (p<0.05)*

Variable		**Healthy (KL=0)**		**Mild KOA (KL=1)**		**Moderate KOA (KL=2)**	
		Ipsilateral	**Contralateral**	**Ipsilateral**	**Contralateral**	**Ipsilateral**	**Contralateral**
Flexion Angle (degrees)	1st	22.1 (0.93)	22.7 (1.22)	**17.5 (1.36) ***	18.0 (2.15)	23.7 (3.93)	22.2 (3.53)
	2nd	37.0 (0.52)	37.1 (0.59)	36.0 (1.33)	36.2 (0.88)	38.3 (1.83)	36.8 (2.06)
Extension Angle (degrees)	1st	-3.78 (0.66)	-4.91 (0.96)	-1.89 (1.51)	-0.54 (1.62)	-5.13 (2.56)	-3.30 (2.66)
	2nd	-6.40 (0.58)	8.77 (0.85)	-4.30 (1.60)	4.90 (1.90)	-7.14 (2.37)	-6.33 (2.32)
Abduction Angle (degrees)	1st	-0.28 (0.47)	-0.76 (0.38)	1.14 (0.99)	-1.42 (1.78)	-0.10 (2.20)	-1.42 (1.78)
	2nd	0.95 (0.55)	-0.14 (0.39)	2.41 (1.03)	1.33 (0.94)	1.46 (1.73)	0.35 (1.56)
Adduction Angle (degrees)	1st	3.39 (0.39)	3.96 (0.38)	1.83 (1.12)	2.86 (0.97)	3.89 (2.04)	4.45 (1.27)
	2nd	2.71 (0.41)	3.18 (0.35)	1.45 (0.99)	1.94 (0.77)	3.08 (1.59)	3.25 (1.43)
Flexion Moment (Nmm/BW)	1st	61.9 (3.49)	68.3 (3.48)	**39.5 (5.32) ****	**48.4 (6.56) ****	73.1 (14.0)	68.1 (14.7)
	2nd	24.6 (1.90)	29.1 (2.05)	25.6 (5.10)	30.0 (3.17)	31.9 (8.92)	27.5 (7.15)
Extension Moment (Nmm/BW)	1st	33.8 (1.97)	30.4 (1.90)	36.4 (4.10)	37.2 (5.09)	19.7 (4.29)	28.2 (7.39)
	2nd	20.8 (2.21)	15.1 (1.90)	29.5 (5.18)	23.7 (3.40)	24.1 (6.55)	22.3 (5.79)
Abduction Moment (Nmm/BW)	1st	37.6 (1.62)	45.9 (1.60)	35.8 (3.16)	40.7 (3.02)	45.5 (12.3)	45.3 (10.3)
	2nd	31.8 (1.72)	39.3 (1.83)	29.2 (3,37)	36.1 (3.11)	40.3 (8.05)	41.9 (8.00)
Adduction Moment (Nmm/BW)	1st	3.94 (0.64)	4.07 (0.56)	4.98 (1.24)	4.59 (1.35)	0.38 (6.66)	-0.22 (6.20)
	2nd	5.53 (0.76)	8.17 (0.63)	7.57 (2.23)	8.93 (1.71)	6.68 (2.96)	4.70 (3.61)
Joint Contact Force (N/BW)	1st	3.39 (0.08)	3.64 (0.07)	**2.92 (0.09) ****	**3.18 (0.15) ****	3.76 (0.50)	3.59 (0.37)
	2nd	3.54 (0.06)	3.54 (0.06)	3.41 (0.09)	3.66 (0.11)	3.47 (0.36)	3.33 (0.27)

*Table 2 - Summary of biomechanical data for OACTIVE subjects stepping showing ipsilateral and contralateral knee joint angles, moments and forces during the first and second half of stance for healthy, mild KOA and moderate KOA subjects. *significantly different to healthy group (p<0.1) ** significantly different to healthy group (p<0.05)*

Variable		**Healthy (KL=0)**		**Mild KOA (KL=1)**		**Moderate KOA (KL=2)**	
		Ipsilateral	**Contralateral**	**Ipsilateral**	**Contralateral**	**Ipsilateral**	**Contralateral**
Flexion Angle (degrees)	1st	77.1 (0.47)	77.7 (0.45)	77.1 (0.92)	78.7 (0.93)	76,7 (2.43)	75.3 (1.60)
	2nd	93.4 (0.79)	91.9 (0.86)	90.5 (2.10)	90.3 (1.74)	93.9 (3.09)	86.6 (3.46)
Extension Angle (degrees)	1st	-33.0 (1.40)	-34.8 (1.52)	-38.3 (2.81)	-37.0 (3.52)	-32.4 (8.29)	-31.4 (4.22)
	2nd	-31.0 (1.40)	-31.7 (1.56)	-34.1 (3.44)	-31.6 (4.17)	-29.4 (7.81)	-26.2 (5.04)
Abduction Angle (degrees)	1st	4.01 (0.90)	1.05 (0.66)	4.22 (1.53)	3.39 (1.31)	1.69 (2.44)	0.26 (2.53)
	2nd	5.26 (0.82)	2.59 (0.56)	5.01 (1.38)	4.65 (1.03)	5.53 (1.72)	2.42 (2.75)
Adduction Angle (degrees)	1st	0.41 (0.79)	3.96 (0.64)	0.89 (1.92)	2.35 (1.45)	2.86 (3.06)	4.51 (2.44)
	2nd	0.49 (0.64)	3.29 (0.54)	-0.60 (1.59)	0.84 (1.17)	0.86 (2.33)	1.93 (2.22)
Flexion Moment (Nmm/BW)	1st	111 (2.89)	107 (2.87)	111 (3.62)	117 (5.69)	130 (5.81)	105 (10.9)
	2nd	175 (3.31)	164 (3.66)	**151 (7.54) ***	156 (7.06)	175 (13.4)	140 (9.02)
Extension Moment (Nmm/BW)	1st	2.56 (0.88)	7.88 (3.85)	3.55 (2.21)	8.11 (3.62)	-4.11 (7.11)	-0.75 (7.74)
	2nd	-35.6 (2.34)	-34.3 (2.53)	-31.0 (5.15)	-31.6 (6.04)	-38.5 (4.07)	-28.8 (6.37)
Abduction Moment (Nmm/BW)	1st	31.9 (1.39)	35.2 (2.73)	29.5 (4.00)	23.3 (4.69)	31.6 (8.12)	27.5 (10.1)
	2nd	31.2 (1.30)	30.5 (2.22)	27.8 (3.94)	**17.7 (5.73) ***	27.5 (5.79)	28.9 (8.23)
Adduction Moment (Nmm/BW)	1st	0.66 (0.97)	0.48 (1.47)	4.45 (2.55)	3.29 (3.06)	6.98 (8.22)	1.14 (8.06)
	2nd	0.23 (0.66)	5.88 (1.32)	2.82 (1.20)	11.4 (3.36)	10.1 (6.03)	3.05 (3.95)
Joint Contact Force (N/BW)	1st	5.36 (0.09)	5.40 (0.08)	5.39 (0.13)	5.58 (0.20)	5.77 (0.23)	5.59 (0.38)
	2nd	4.77 (0.12)	4.43 (0.12)	**4.15 (0.27) ***	4.36 (0.28)	4.89 (0.48)	4.00 (0.21)

3.4 Summary

This study compares knee joint kinematics and kinetics between healthy subjects and those with mild or moderate knee osteoarthritis. Significant alterations in knee joint kinematics were seen in subjects with mild KOA during gait with a reduction in the amount of flexion during the first half of stance in the affected limb. This stiffening of the knee during loading is likely to be a coping strategy employed to reduce loading in the knee, and it can be seen here that it has such an effect. There was evidence that subjects with more mild disease had reduced knee joint loading and knee flexion moments, particularly during the 1^{st} half of the stance phase during walking where flexion angles were also reduced. This study has not looked at joint forces or moments in other joints, but it is likely that the alterations seen at the knee may lead to altered biomechanics at the hip and ankle. Similar reductions in peak loading and flexion moments were seen in mild KOA subjects undergoing stepping movements, however these did not correspond with reduced flexion angles at the knee in the same way as during gait. This may suggest other kinematic strategies to reduce joint loading during stepping that are not immediately obvious here.

Interestingly, this coping strategy seen in subjects with mild KOA is not seen in those with more severe forms of the diseases. It should be noted that the number of subjects with more severe KOA was much smaller than the other sample groups, making any changes harder to detect. It is also the case that those subjects in general had a lot more variation in a lot of the variables measured than the other sample groups, again making any overall changes harder to detect statistically. It may also be the case that the coping mechanisms employed by subjects with mild KOA either do not work as well in subjects with more severe disease or the subjects are unable to carry out such movements due to other restrictions in movement or increased pain. Further studies are required to isolate any possible reasons for these findings and the OACTIVE dataset provides a great tool for future studies to investigate these areas and many more.

4 Effect of meniscus inclusion and flexion angle on predicted cartilage mechanics in healthy knees

4.1 Introduction

The inclusion of menisci into the finite element models developed as part of this project significantly increases the complexity and computing time of the models. Several previous studies using FE models of the knee have removed the menisci in order to reduce the complexity of the models, but it is unclear how justifiable this is, or to what extent the menisci affect the distribution of tissue stresses in these models. This is particularly relevant in KOA subjects, where altered meniscal morphology often coincides with other damage to the joint and may be an important aspect to consider when trying to develop subject specific models of their knees. Incorporating flexion angles into an FE model of the knee also greatly increases complexity, both computationally and experimentally, however it is not known the degree to which the flexion angle affects cartilage stresses under fixed loads. Whilst compressive loading can reasonably be scaled based on weight to avoid needing subject specific joint loading information, there is no reasonable way to scale flexion angles between different subjects. The only way to generate flexion angles for each subject is to measure them experimentally via gait analysis methods. These can be very difficult and time consuming to carry out and is often not feasible. This is particularly the case when dealing with existing datasets where gait analysis was not carried out. Because of this, several studies have used generic joint flexion angles to build and simulate gait in phenotypically different groups such as those with and without knee osteoarthritis. Subjects with knee osteoarthritis are known to have significantly different flexion angles during peak loading and the results and so the use of generic joint angles may not be inappropriate. This study aims to understand the importance of including the menisci and/or the inclusion of subject specific joint angles. It will do this by evaluating the variation in cartilage stresses in healthy subjects caused by the inclusion of menisci and the variation of flexion angle.

4.2 Methods

In order to evaluate the effect of menisci on tissue stresses, two FE models of a healthy knee based on MR geometry were developed. One of these models included the menisci and one was constructed without the menisci present (Figure 8). A gradual vertical 2500N compressive load was applied to each model at a series of flexion angles ranging from 5 to 20 degrees. These angles were chosen as they represent the range of flexion angles that would be likely at the point of peak loading during gait. Compressive stresses, shear stresses and contact areas acting on the medial and lateral sides of the tibial and femoral cartilage were extracted after the simulations had run. The difference in these variables between the simulation with the menisci and the one without were calculate and plotted.

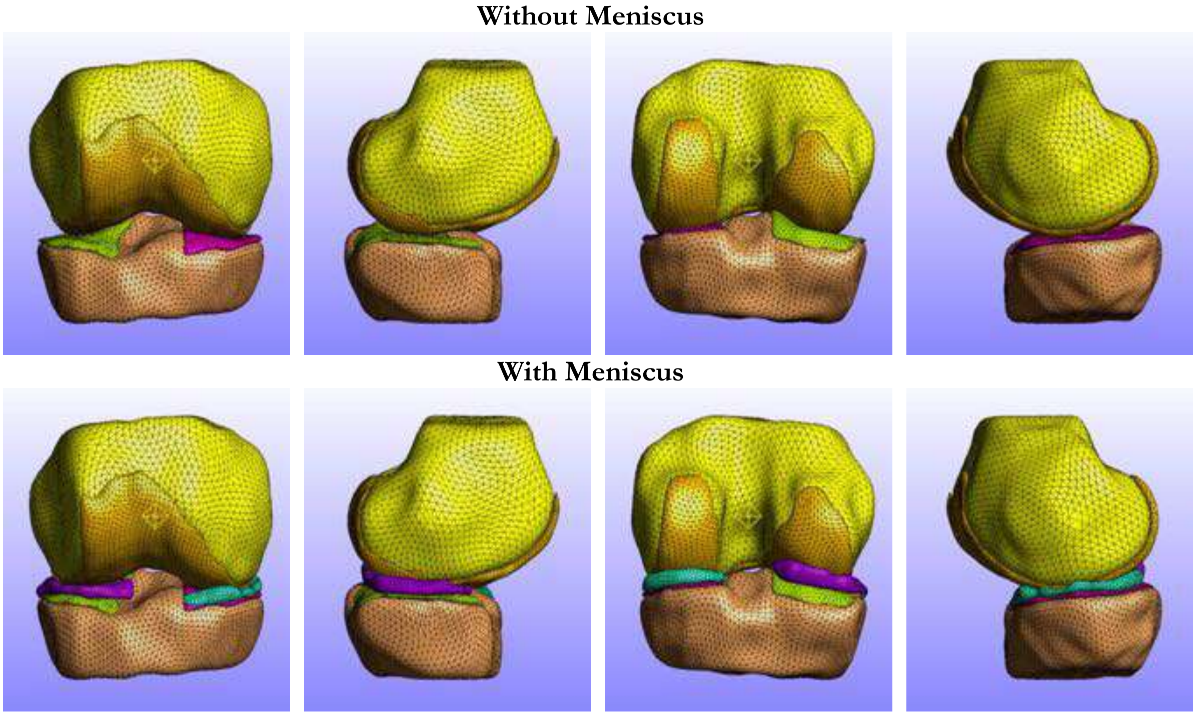

Figure 8 - Three dimensional meshed reconstructions of subjects knee joint with and without menisci. Tissues are colour labelled and comprise of the tibia, femur, medial tibial cartilage, lateral tibial cartilage, femoral cartilage, medial meniscus and lateral meniscus

4.3 Results

Compressive Stresses

Figure 10 and Figure 11 show the distribution of compressive stresses on the femur and tibia respectively at 5, 10, 15 and 20 degrees of flexion for the model with menisci and the model without. It can be seen visually that the general pattern of stress distribution is fairly similar between the two models. Stresses tend to increase, and the location of peak stresses move in the anterior direction as the flexion angle increases. The locations of these peak stresses are fairly similar between the two models, but the magnitude appears to be increased in the tibial and femoral components for the model without the menisci. Figure 9 shows the quantitative outputs from the finite element models. It can be seen that in the medial and lateral tibial cartilage, peak cartilage stresses increase with increasing flexion with or without menisci. The removal of menisci increases the peak compressive stress at all flexion angles, but the degree to which it is increased does vary somewhat, with the effect being more pronounced in the lateral component. At 5 degrees flexion for example, the model without menisci experienced 28% larger compressive stresses in the lateral compartment as supposed to 10% larger in the medial compartment when compared to the model with menisci. The peak compressive stresses in the femoral component also increased with increasing flexion in both models.

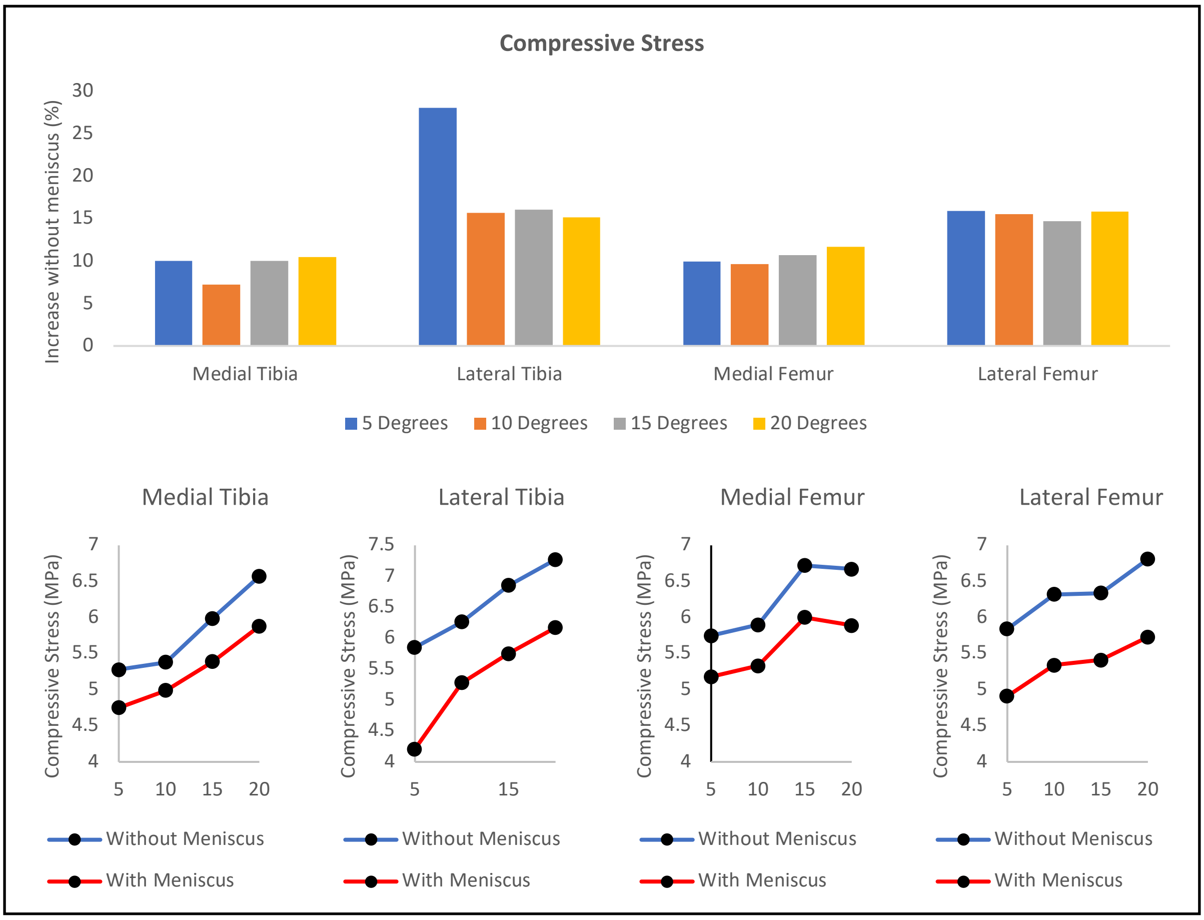

Figure 9 - Effect of flexion angle and the presence of menisci on peak compressive stresses in femoral and tibial cartilage. Top: Bar chart showing the increase in peak compressive stresses that occur in the model without menisci for each of the cartilage components at each flexion angle. Bottom: Line graphs showing how peak compressive stress changes with flexion angle in the tibial and femoral components as well as how it is affected by the presence of menisci

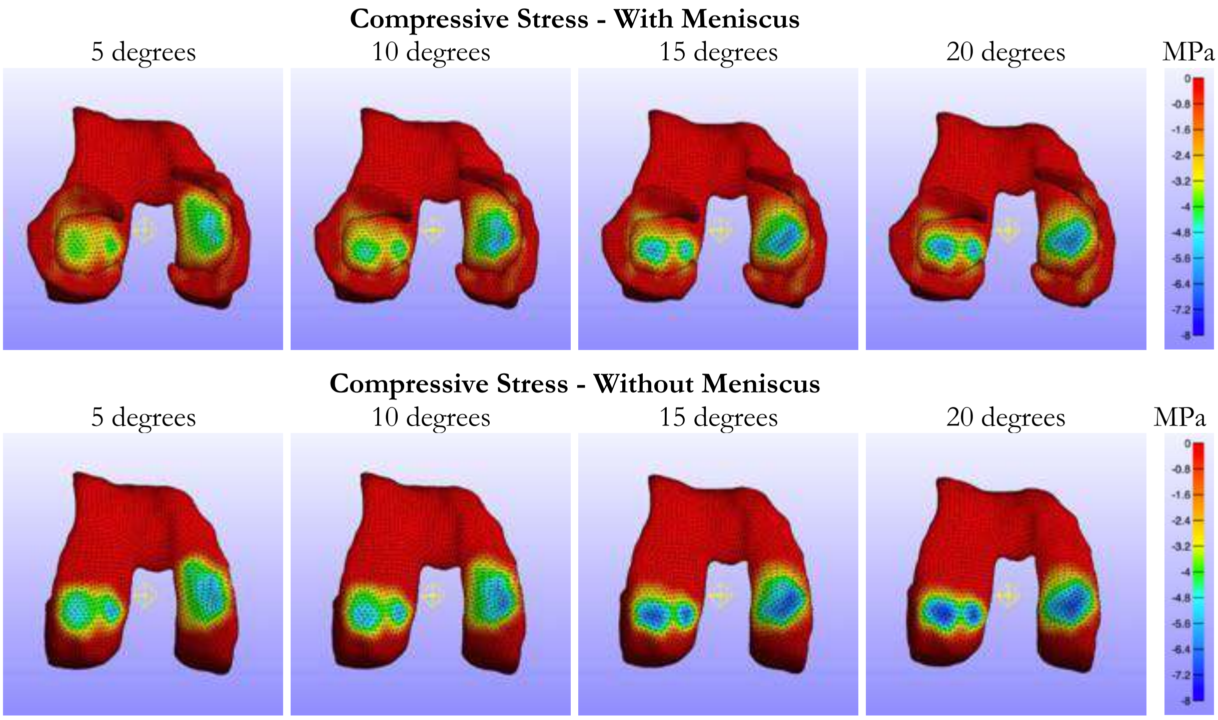

Figure 10 - Compressive stress on the femoral cartilage of a healthy subject undergoing 2500N of compressive loading at flexion angles between 5 and 20 degrees. Lateral side is shown on the left and medial on the right

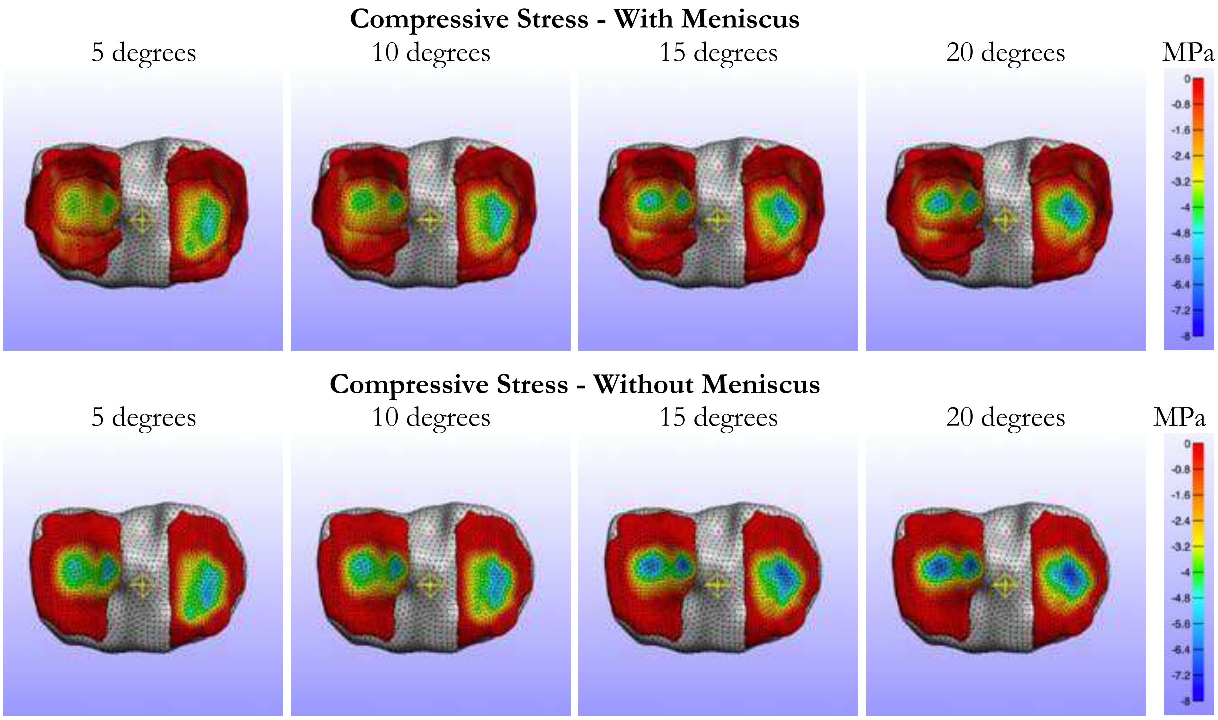

Figure 11 - Compressive stress on the tibial cartilage of a healthy subject undergoing 2500N of compressive loading at flexion angles between 5 and 20 degrees. Lateral side is shown on the left and medial on the right

Shear Stresses

Figure 13 and Figure 14 show visually the distribution of shear stresses on the femoral and tibial cartilage at varying flexion angles in subjects with and without menisci. As with the compressive stress, the pattern of loading appears consistent between the two models, with the areas of peak shear stresses corresponding closely to the areas of peak compressive stress discussed earlier. The quantitative findings, shown in Figure 12 are very similar to those reported for compressive stresses.

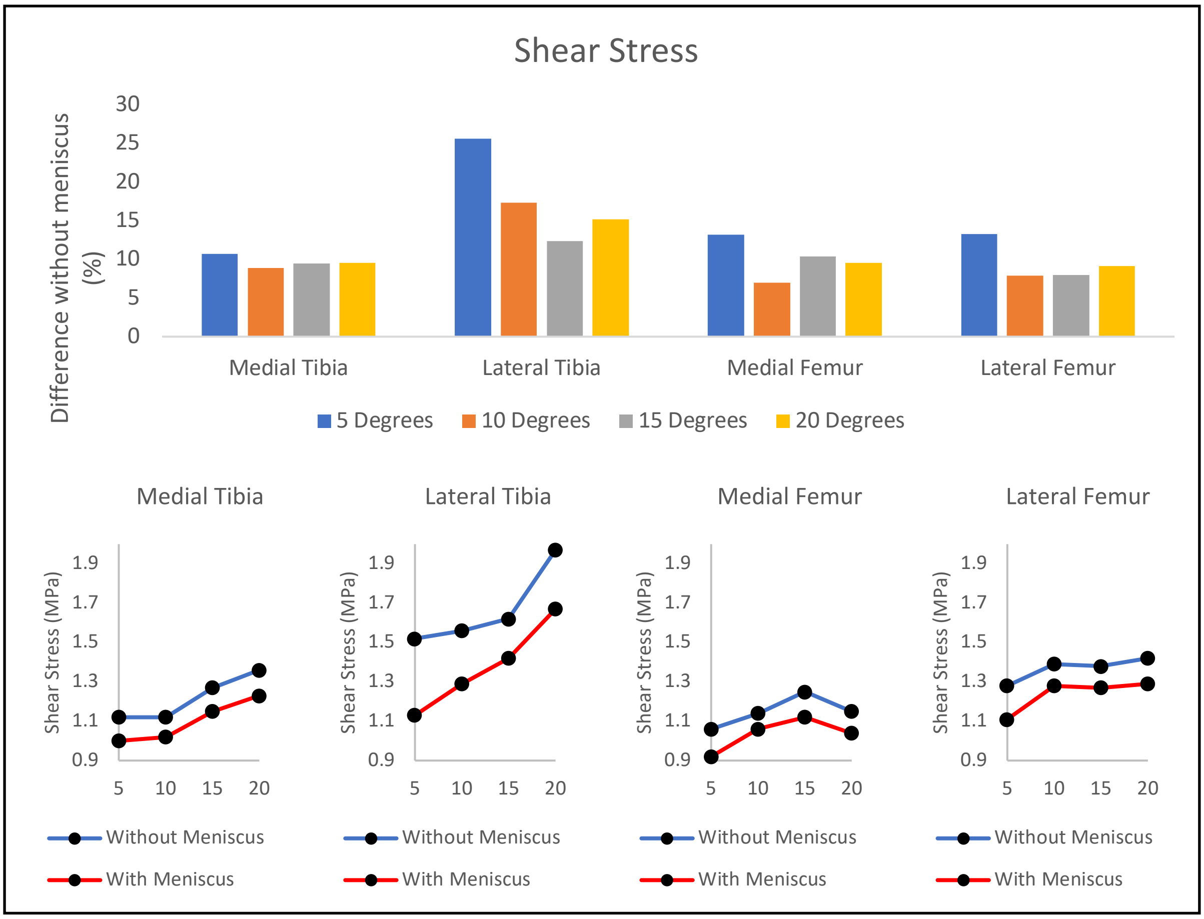

Figure 12 - Effect of flexion angle and the presence of menisci on peak shear stresses in femoral and tibial cartilage. Top: Bar chart showing the increase in peak shear stresses that occur in the model without menisci for each of the cartilage components at each flexion angle. Bottom: Line graphs showing how peak shear stress changes with flexion angle in the tibial and femoral components as well as how it is affected by the presence of menisci

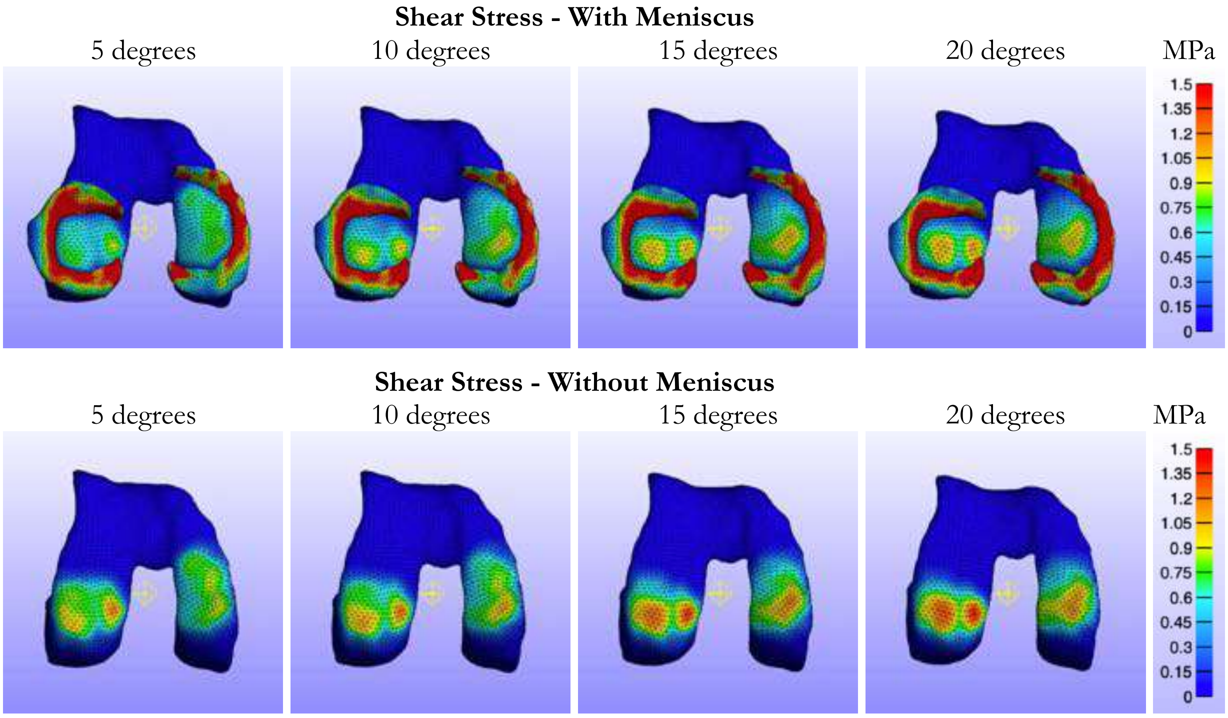

Figure 13 - Shear stress on the femoral cartilage of a healthy subject undergoing 2500N of compressive loading at flexion angles between 5 and 20 degrees. Lateral side is shown on the left and medial on the right

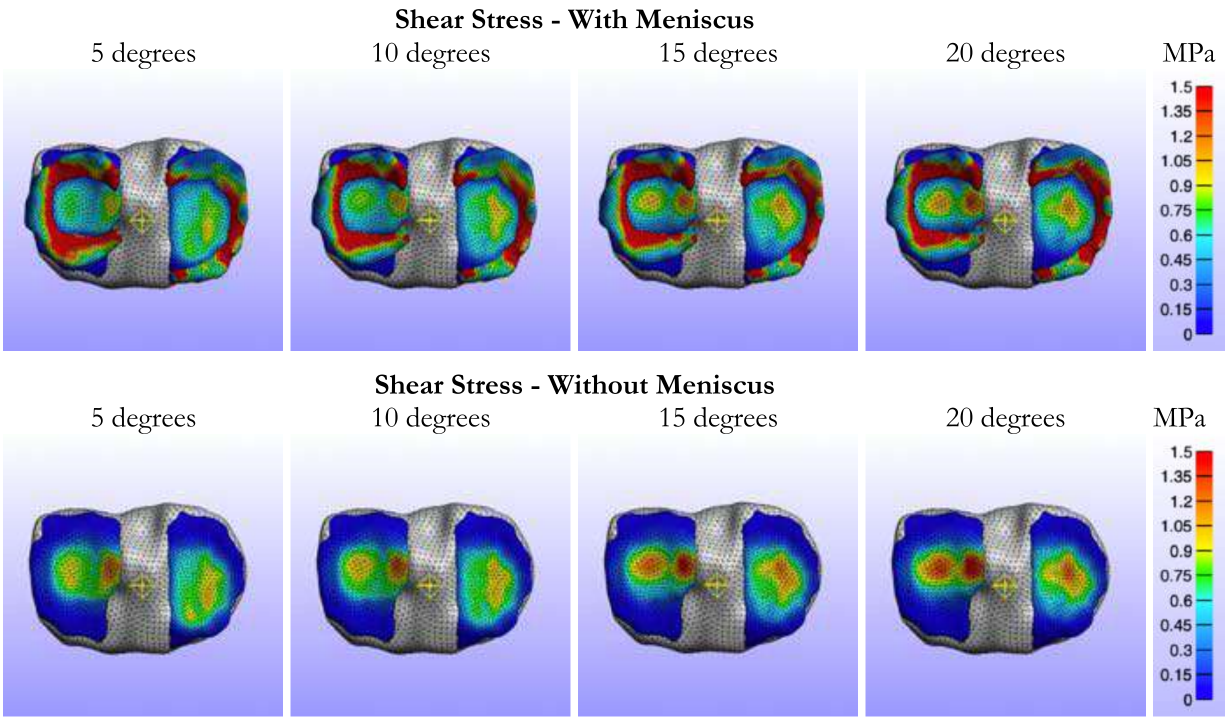

Figure 14 - Shear stress on the tibial cartilage of a healthy subject undergoing 2500N of compressive loading at flexion angles between 5 and 20 degrees. Lateral side is shown on the left and medial on the right

Contact Area

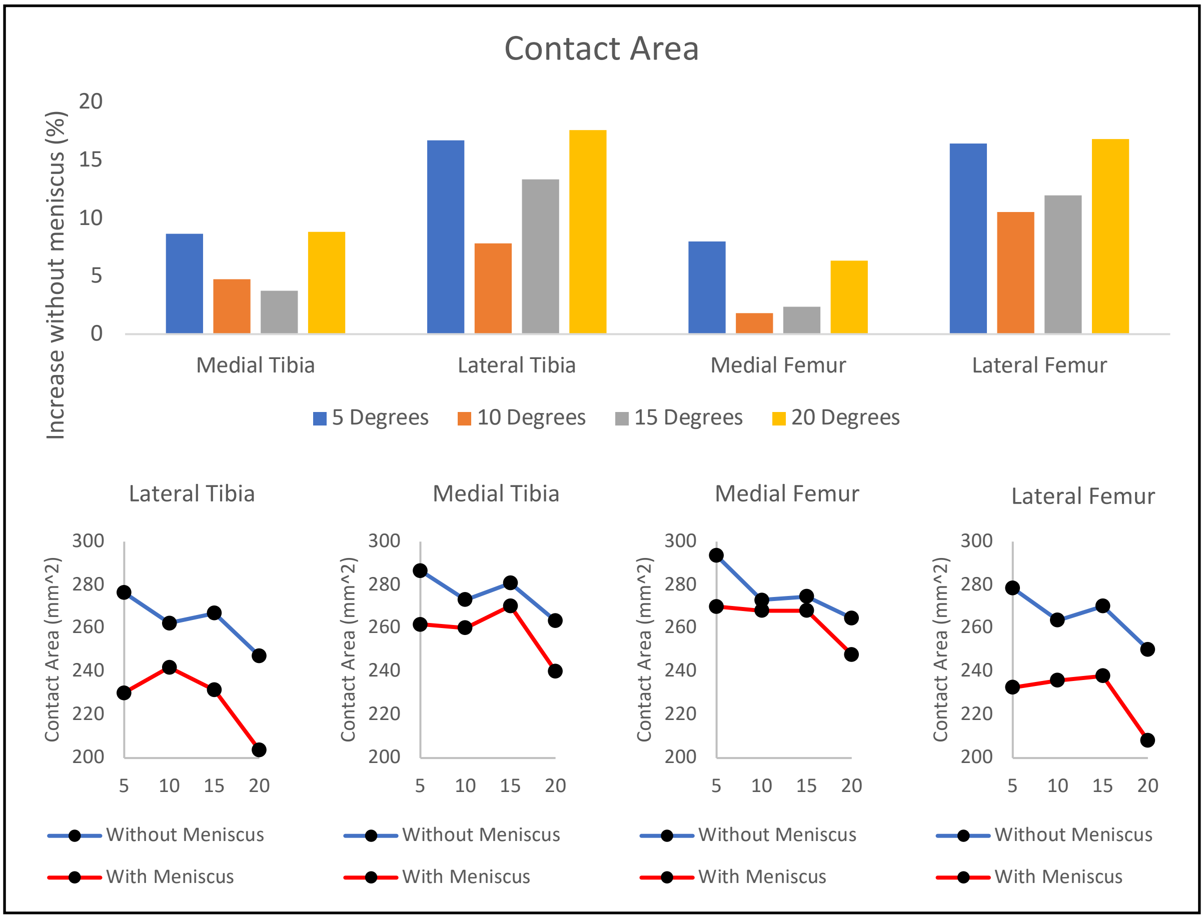

Figure 15 - Effect of flexion angle and the presence of menisci on contact areas in femoral and tibial cartilage. Top: Bar chart showing the increase in contact area that occurs in the model without menisci for each of the cartilage components at each flexion angle. Bottom: Line graphs showing how contact area changes with flexion angle in the tibial and femoral components as well as how it is affected by the presence of menisci

Figure 15 shows how the contact areas on the femoral and tibial cartilage vary with and without menisci at flexion angles between 5 and 20 degrees. Contact areas were seen to reduce as the flexion angle increased in all compartments of the tibial and femoral cartilage. As might be expected, contact areas are seen to be greater in subjects without the menisci, illustrating the key role that the menisci play in directing and constraining the areas of the cartilage that are subjected to peak loading. The effect of the menisci is more pronounced on the lateral side of the knee than in the medial side.

This is likely to be due to the geometry of the menisci, where the lateral menisci form a tighter radius and thus restrict the contact areas more than the medial menisci. The effect of the menisci is quite variable and appears to depend heavily on the flexion angle. In general the menisci appear to restrict the contact areas more greatly at the extreme ends of the flexion range (5 and 20 degrees) and have less of an effect in the moderate ranges.

Quantitative Results

		5 degrees		10 degrees		15 degrees		20 degrees	
		Without	With	Without	With	Without	With	Without	With
Medial Tibia	Z stress	5.28	4.75	5.38	4.99	5.99	5.39	6.57	5.88
	Shear Stress	1.12	1	1.12	1.02	1.27	1.15	1.36	1.23
	Contact Area	287	262	273	260	280	270	263	240
Lateral Tibia	Z stress	5.85	4.21	6.26	5.28	6.85	5.75	7.27	6.17
	Shear Stress	1.52	1.13	1.56	1.29	1.62	1.42	1.97	1.67
	Contact Area	276	230	262	241	267	231	247	203
Medial Femur	Z stress	5.75	5.18	5.9	5.33	6.72	6	6.67	5.89
	Shear Stress	1.06	0.92	1.14	1.06	1.25	1.12	1.15	1.04
	Contact Area	293	270	273	268	274	268	264	247
Lateral Femur	Z stress	5.84	4.91	6.32	5.34	6.34	6.2	6.81	7.21
	Shear Stress	1.28	1.11	1.39	1.28	1.38	1.87	1.42	1.94
	Contact Area	278	232	263	235	270	237	250	208

4.4 Summary

In general, the pattern of loading for all metrics is quite similar between the two models, indicating that even simple models without menisci can be used under some circumstances. The differences between the two models are fairly consistent under most loading conditions, with the menisci acting to reduce the contact area on the cartilage and reduce peak stresses. If these variations are consistent amongst subjects as well as within subjects, as displayed here, then it is likely that comparisons between phenotypically distinct subgroups would still be valid with simplified models even if the quantified outputs are not as accurate. It should be noted, however, that even within the one subject studied here, there were large variations in how the menisci affected certain variables. In the lateral tibia, for instance, the increase in stresses seen in the model without menisci are much larger at some flexion angles than others. Although this doesn't affect the overall trend of increased stresses at increased angles, it could make comparisons between subjects difficult without modelling the effect of the menisci. Caution however, should be taken in assuming that removing the menisci affects all samples in the same way. Osteoarthritic subjects are known to often have meniscal damage in conjunction with the other joint damage present in the knee. Altered meniscal morphology likely reduces the degree to which the menisci are able to reduce cartilage stresses in this healthy subject. In this case, removing the menisci may increase stresses in healthy subjects and not those with impaired meniscal morphology, reducing or removing any increase in cartilage stress that may be expected in the osteoarthritic subject. Further study with osteoarthritic subjects is required to evaluate this.

5 Effect of Age and Incidence of KOA on Cartilage Loading

5.1 *Introduction*

This section includes a summary of the six subject specific finite element models developed as part of WP3.1

5.2 *Methods*

In order to investigate the effect of Incident KOA on the strains and stresses experienced in the cartilage, subject specific finite element models were constructed for six subjects using the methods described earlier in this report and in more detail in D3.1. The six subjects were chosen randomly from the OACTIVE dataset and comprised of the following:

- Young healthy male (YHM)
- Young healthy female (YHF)
- Older healthy male (EHM)
- Older healthy female (EHF)
- Older Osteoarthritic male (EOM)
- Older Osteoarthritic female (EOF)

Young was defined as between 18 and 25 years old, with older being defined as being over 50 years old. Incidence of KOA was identified via KL score. A description of the characteristics of theses subjects, including their age, weight, BMI and KL score can be found in Table 3 below:

	Young healthy male	**Young healthy female**	**Older healthy male**	**Older healthy female**	**Older osteoarthritic male**	**Older osteoarthritic female**
Label	YHM	YHF	EHM	EHF	EOM	EOF
Age (yrs)	32	18	56	59	50	64
Weight (kg)	74.0	65	89.5	66	85	64.5
Height (m)	1.74	1.66	1.79	1.585	1.76	1.56
BMI	24.4	23.6	27.9	26.3	27.44	26.5
KL	0	0	0	0	2	1

Table 3 - Characteristics of subjects selected for construction of subject specific models

Each of the subjects' models was subjected to two simulations, to simulate the first and second peaks of compressive loading in the knee. The joint contact forces at the knee in all three axis were extracted at the locations of the first and second peaks of compressive contact force. The flexion angles were also extracted at the same location. For each of these time points the models were flexed to the appropriate flexion angle under a small vertical load and were then loaded gradually up to the maximum loading in all three axis. Compressive stresses, shear stresses and contact areas acting on the medial and lateral sides of the tibial were extracted after the simulations had run.

5.3 Results

Figure 16 shows the subject specific finite element models for the six subjects in 4 different orthographic projections. It can be seen that, at least in these views, there is not a large difference in external geometry between the subjects, although there are of course subject specific morphological variations. The main difference between the subjects is the reduced cartilage thickness and altered meniscal morphology seen in the osteoarthritic female in particular.

The tibial compressive stresses (Figure 17) and strains (Figure 21) at first peak loading were investigated and there were differences found between the groups of subjects. Average stresses on the medial and lateral tibial cartilage in the younger healthy groups (medial: 4.25MPa, lateral: 3.56MPa) were lower than those seen in older healthy (medial: 4.29MPa, lateral: 5.01MPa) or older osteoarthritic subjects (medial: 8.73MPa, lateral: 8.62MPa). This is a large increase in the osteoarthritic group and can be seen visually in the pressure distributions with large blue areas of increased stresses in the osteoarthritic subjects. Tibial strains followed similar trends, with older osteoarthritic subjects having higher tibial cartilage strains (33-42%) than older healthy (23-29%) or younger healthy (23-28%) subjects. Increased stresses in the tibia at the second peak JCF were also elevated in osteoarthritic groups, but the increases were less obvious than at the first peak (Figure 19). The younger healthy female also had higher stress at the second peak in the medial compartment than would be expected and this needs further investigation to see if this is an anomaly or something present in more subjects. The strains at second peak loading in the tibial cartilage were in general higher in the osteoarthritic group, however there were high strains also present in the older healthy male and younger healthy female subjects (Figure 23).

Femoral stresses and strains were also investigated and although there were still differences between the subjects they were less pronounced than those seen in the tibia (Figure 18). At first peak loading the average peak stresses seen in the femoral cartilage were higher in the osteoarthritic groups (medial: 5.85MPa, lateral: 7.6MPa) than in the older healthy (medial: 5.4MPa, lateral: 5.27MPa) or younger groups (medial: 4.12MPa, lateral: 4.39MPa). Strains at first peak loading were also slightly higher in osteoarthritic subjects and the areas of peak strain appear to extend more widely across the surface of the femur (Figure 22). Stresses at second peak loading do not appear to vary as much between the subjects, with the stresses in the osteoarthritic subjects reducing significantly compared to those seen at first peak loading. The same is true with the peak strain on the femur at second peak, with most subjects experiencing strains of between 23% and 27%.

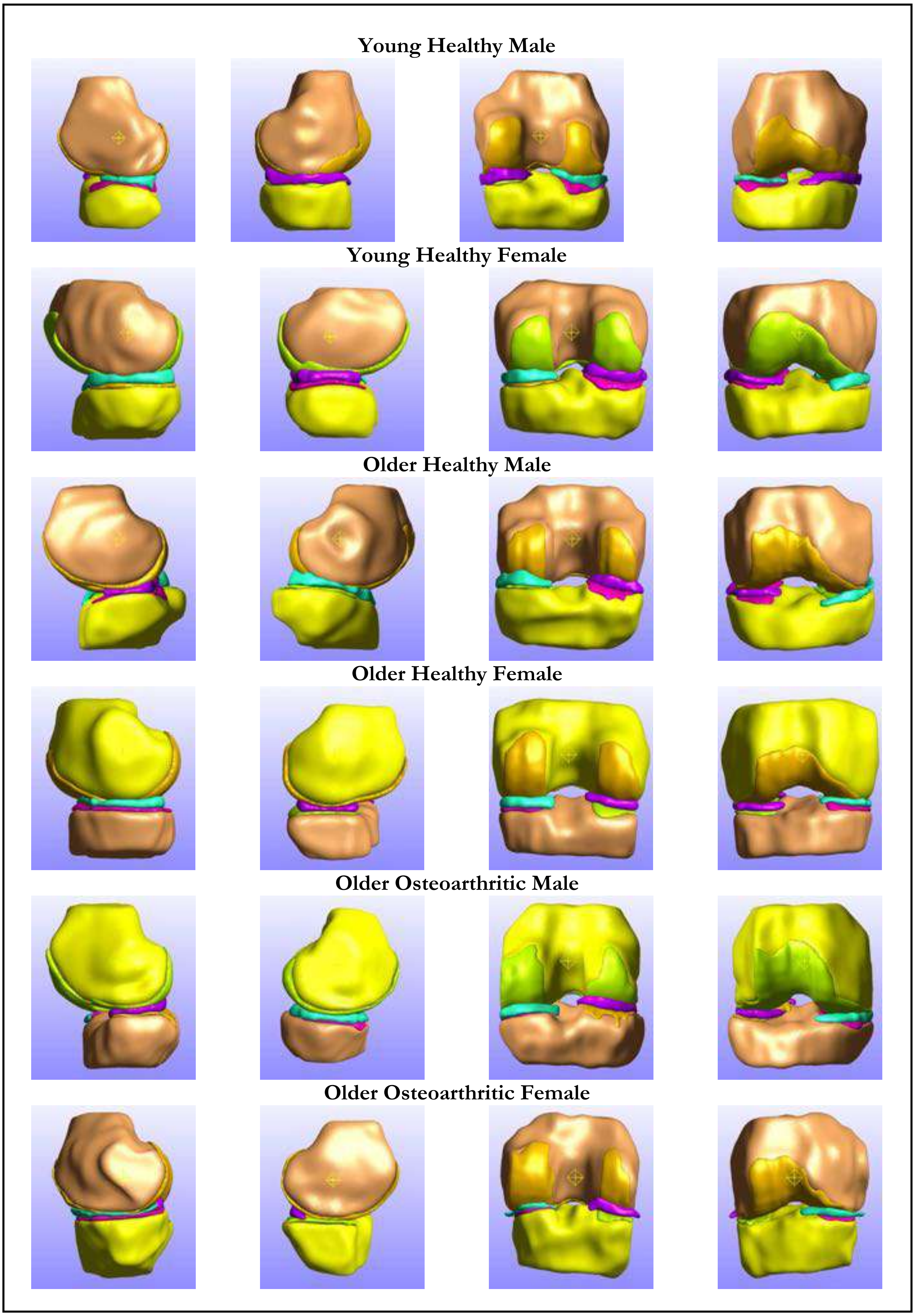

Figure 16 - Subject specific finite element models of six subjects using segmented geometries of the femur, tibia, femoral cartilage, tibial cartilage and menisci

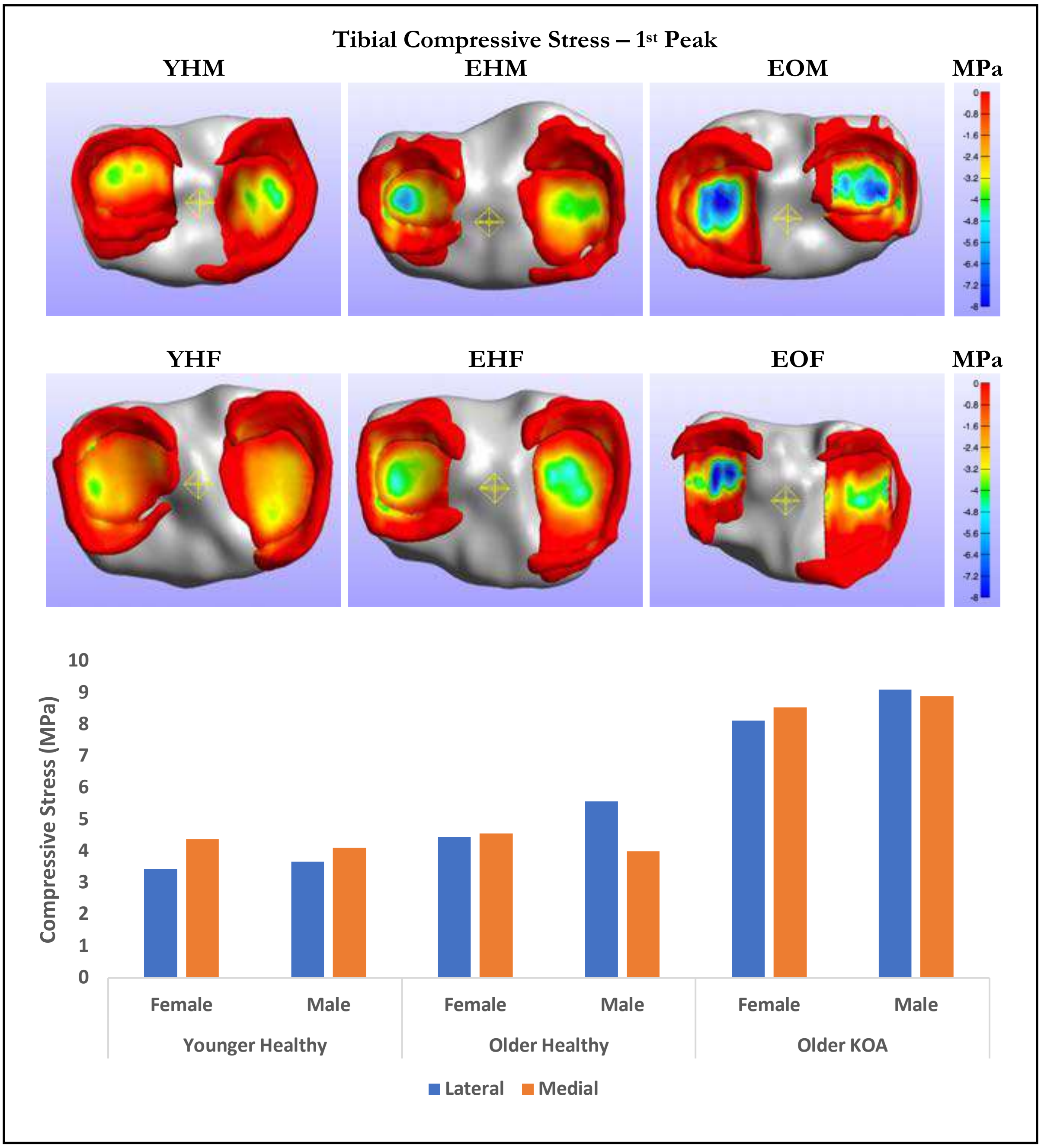

Figure 17 - Compressive stress on the tibia at the 1st peak joint contact force. Top: Visual representation of strain distribution across the cartilage surface. Bottom: Bar chart showing peak cartilage strains

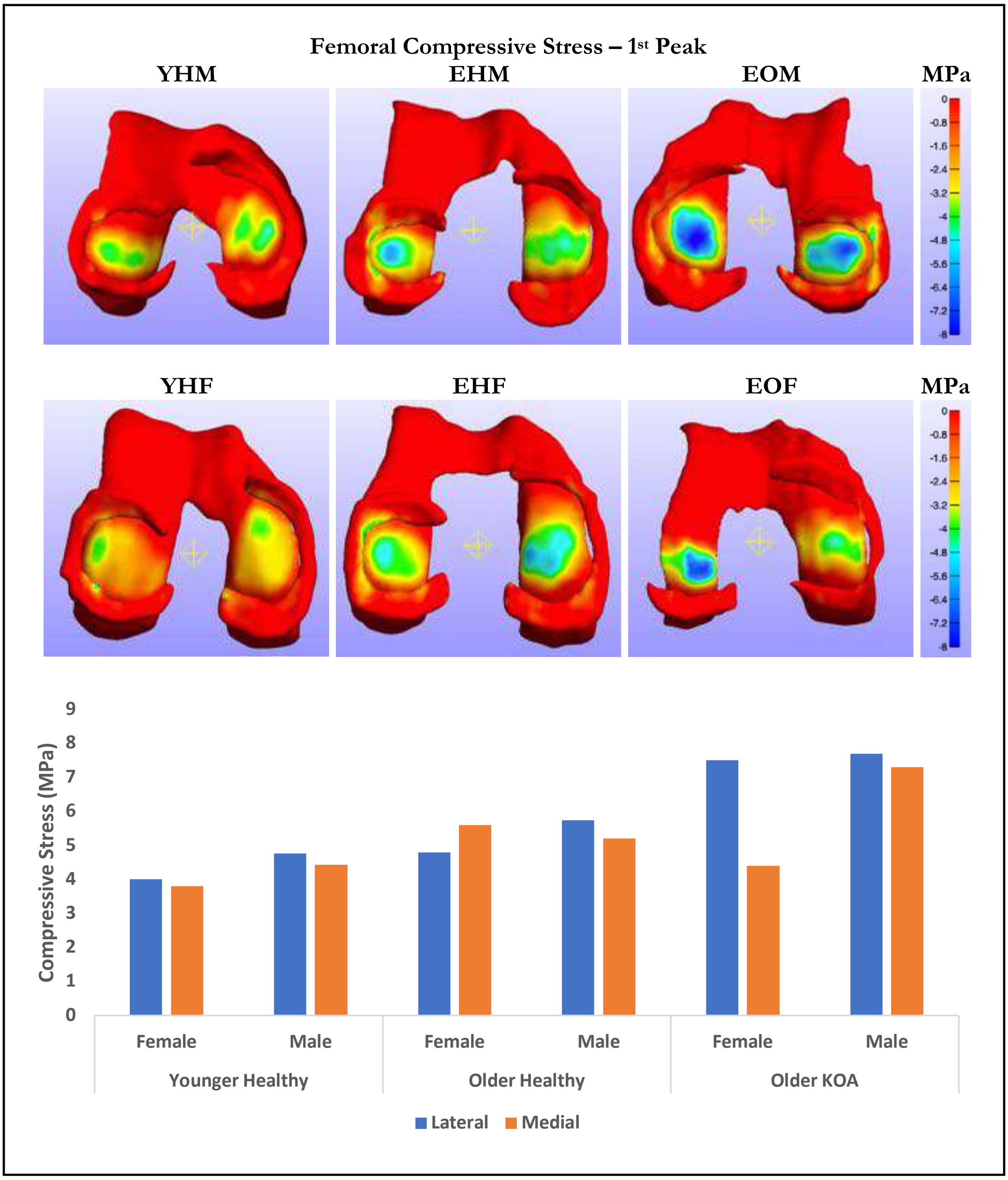

Figure 18 - Compressive stress on the femur at the 1st peak joint contact force. Top: Visual representation of strain distribution across the cartilage surface. Bottom: Bar chart showing peak cartilage strains

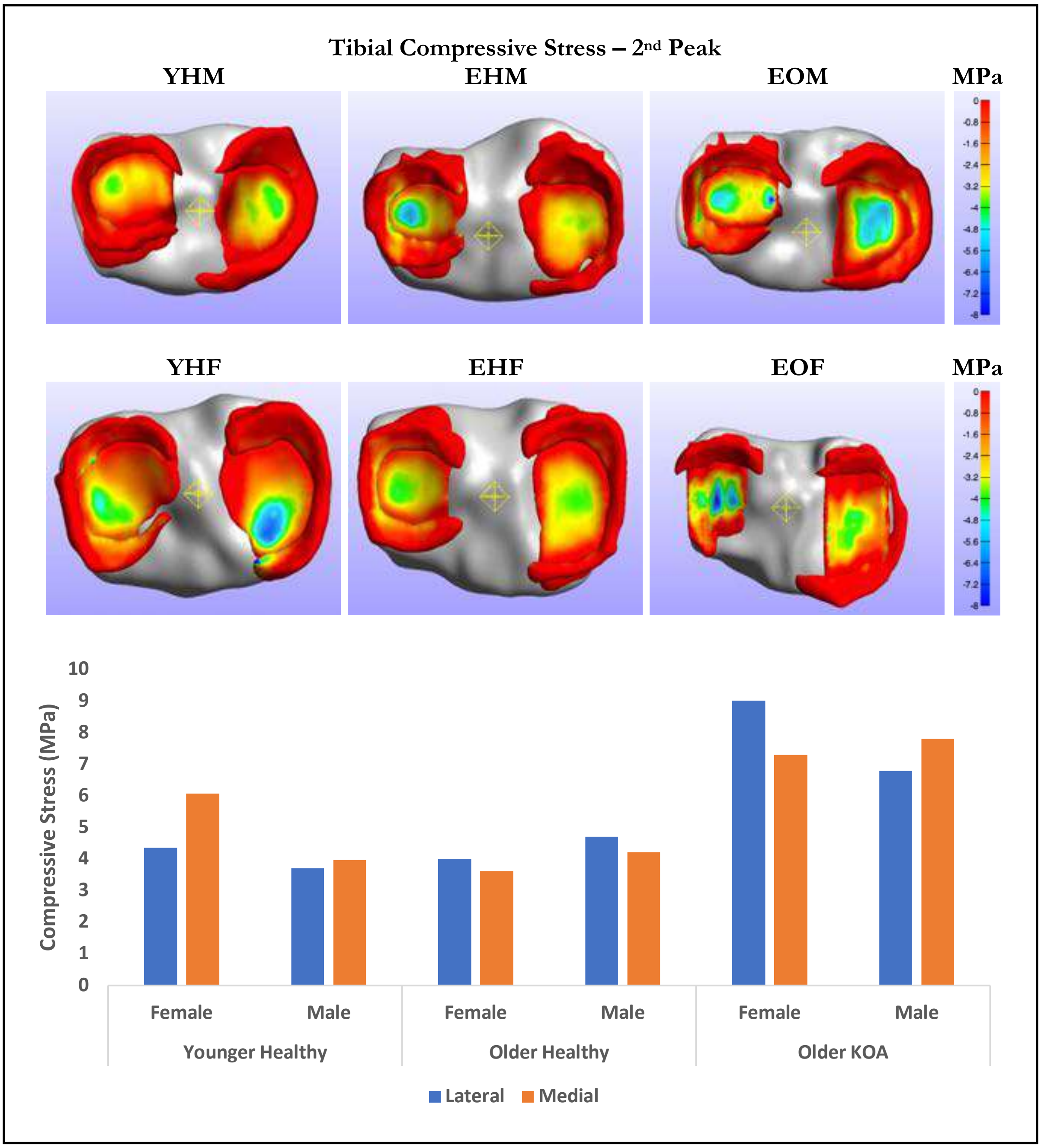

Figure 19 - Compressive stress on the tibia at the 2nd peak joint contact force. Top: Visual representation of strain distribution across the cartilage surface. Bottom: Bar chart showing peak cartilage strains

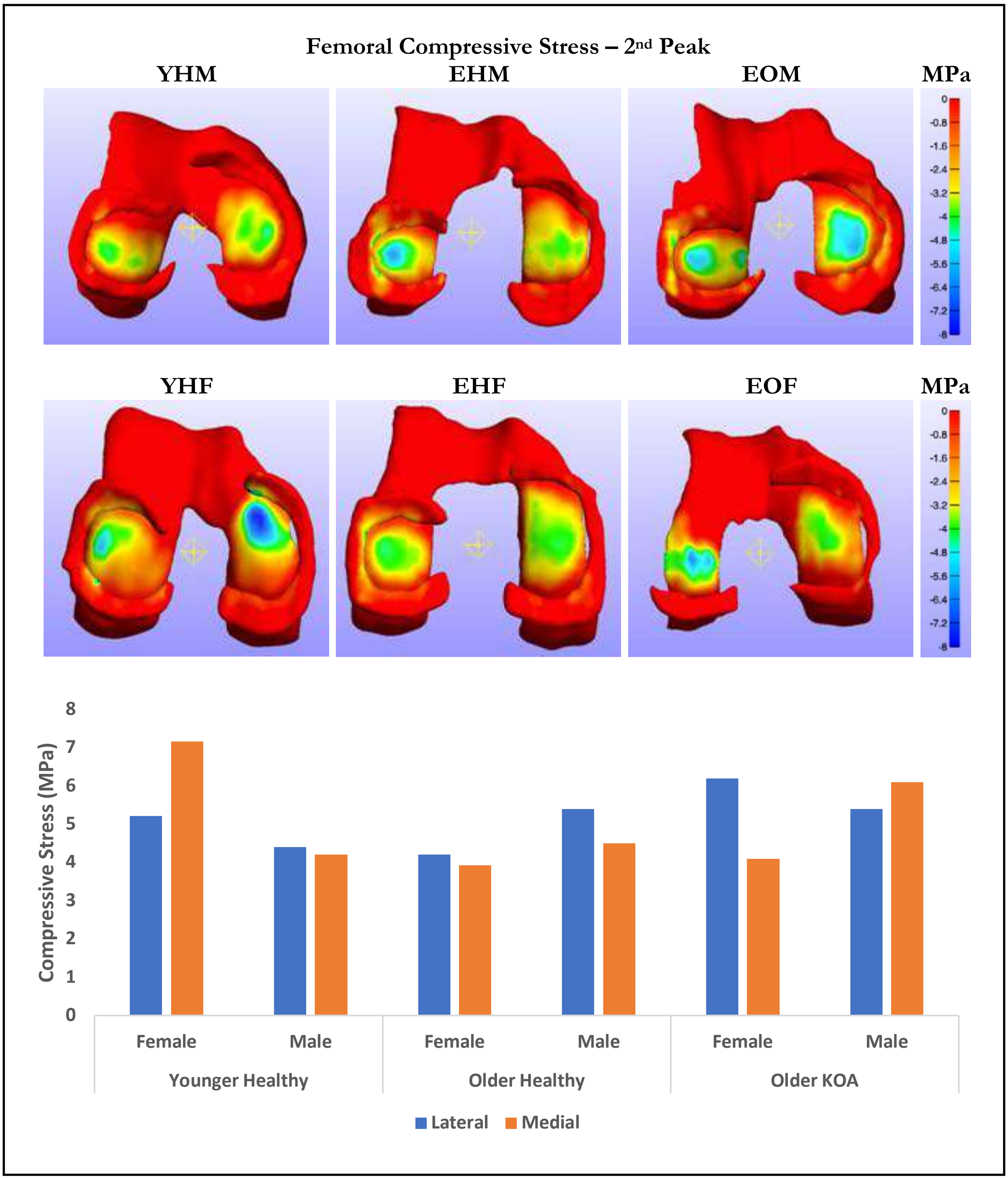

Figure 20 - Compressive stress on the femur at the 2nd peak joint contact force. Top: Visual representation of strain distribution across the cartilage surface. Bottom: Bar chart showing peak cartilage strains

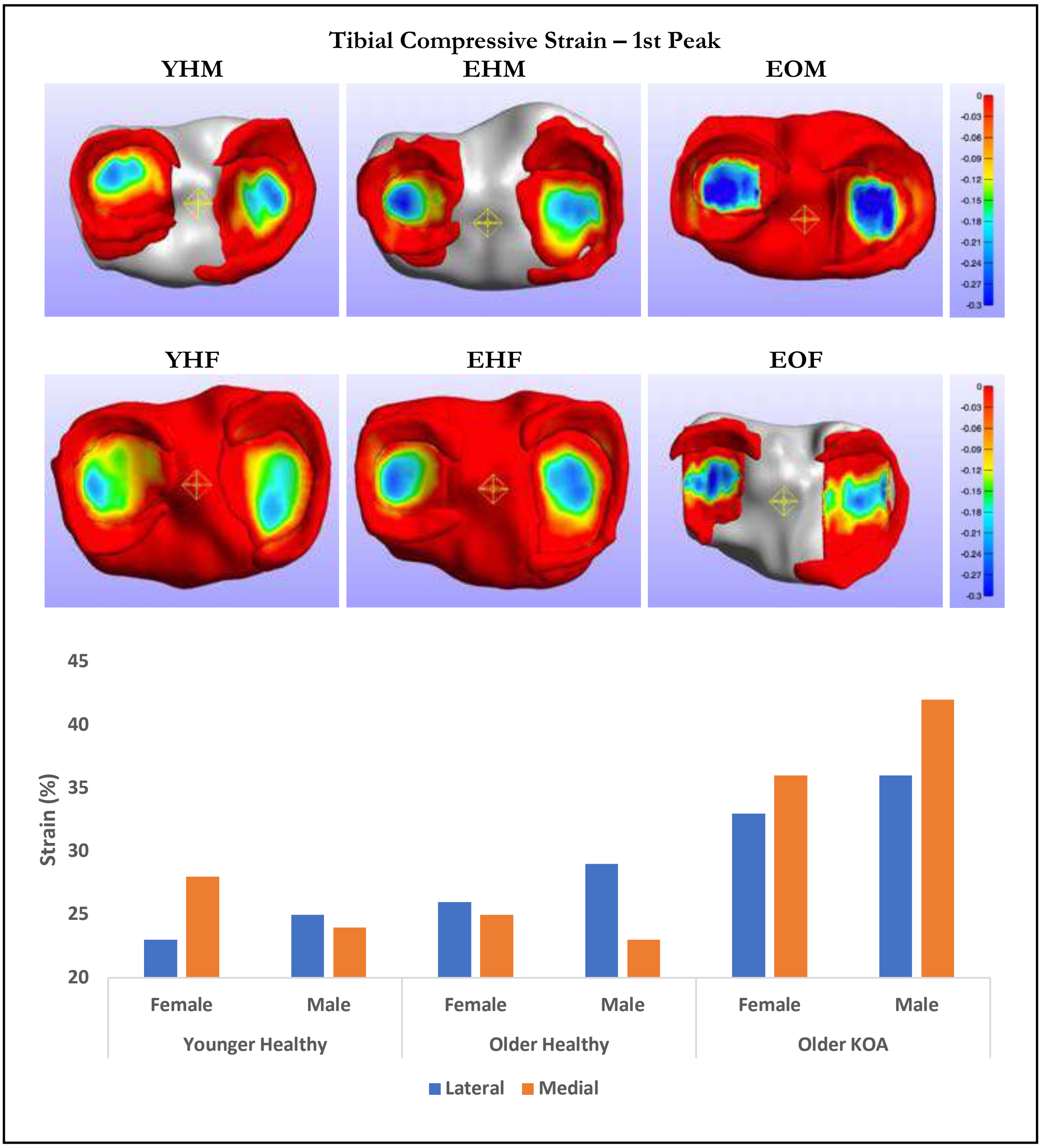

Figure 21 - Compressive strain on the tibia at the 1st peak joint contact force. Top: Visual representation of strain distribution across the cartilage surface. Bottom: Bar chart showing peak cartilage strains

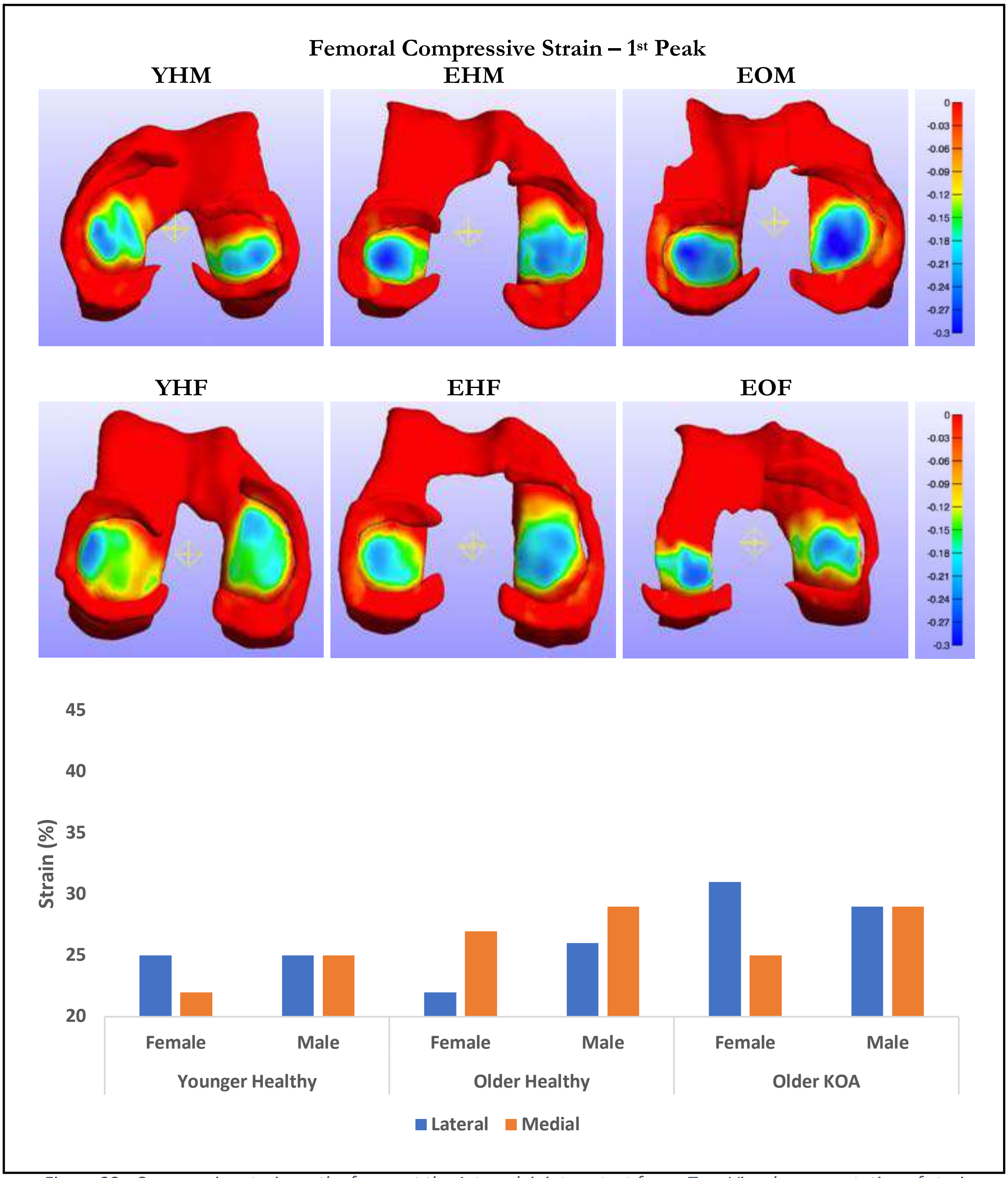

Figure 22 - Compressive strain on the femur at the 1st peak joint contact force. Top: Visual representation of strain distribution across the cartilage surface. Bottom: Bar chart showing peak cartilage strains

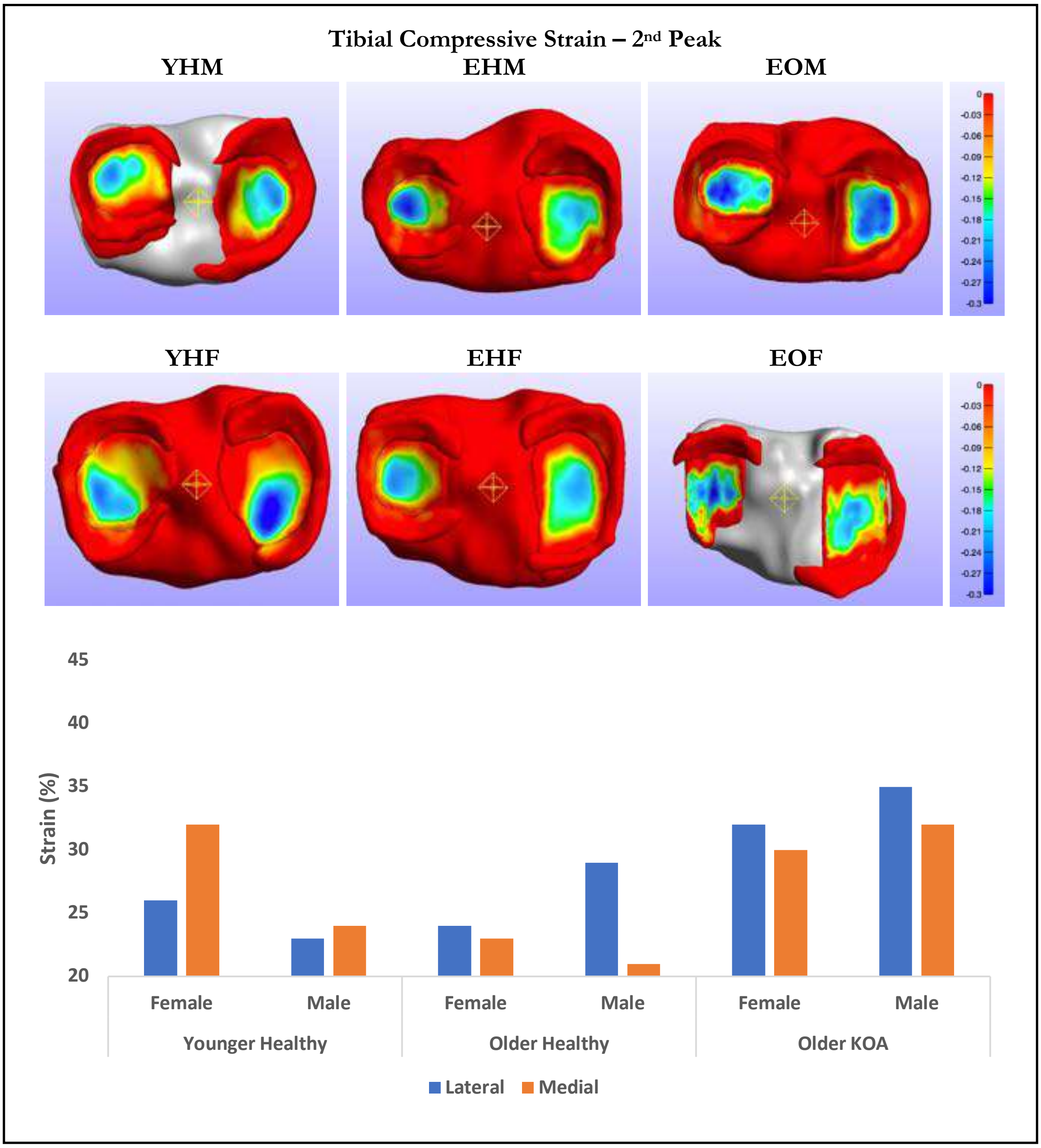

Figure 23 - Compressive strain on the tibia at the 2nd peak joint contact force. Top: Visual representation of strain distribution across the cartilage surface. Bottom: Bar chart showing peak cartilage strains

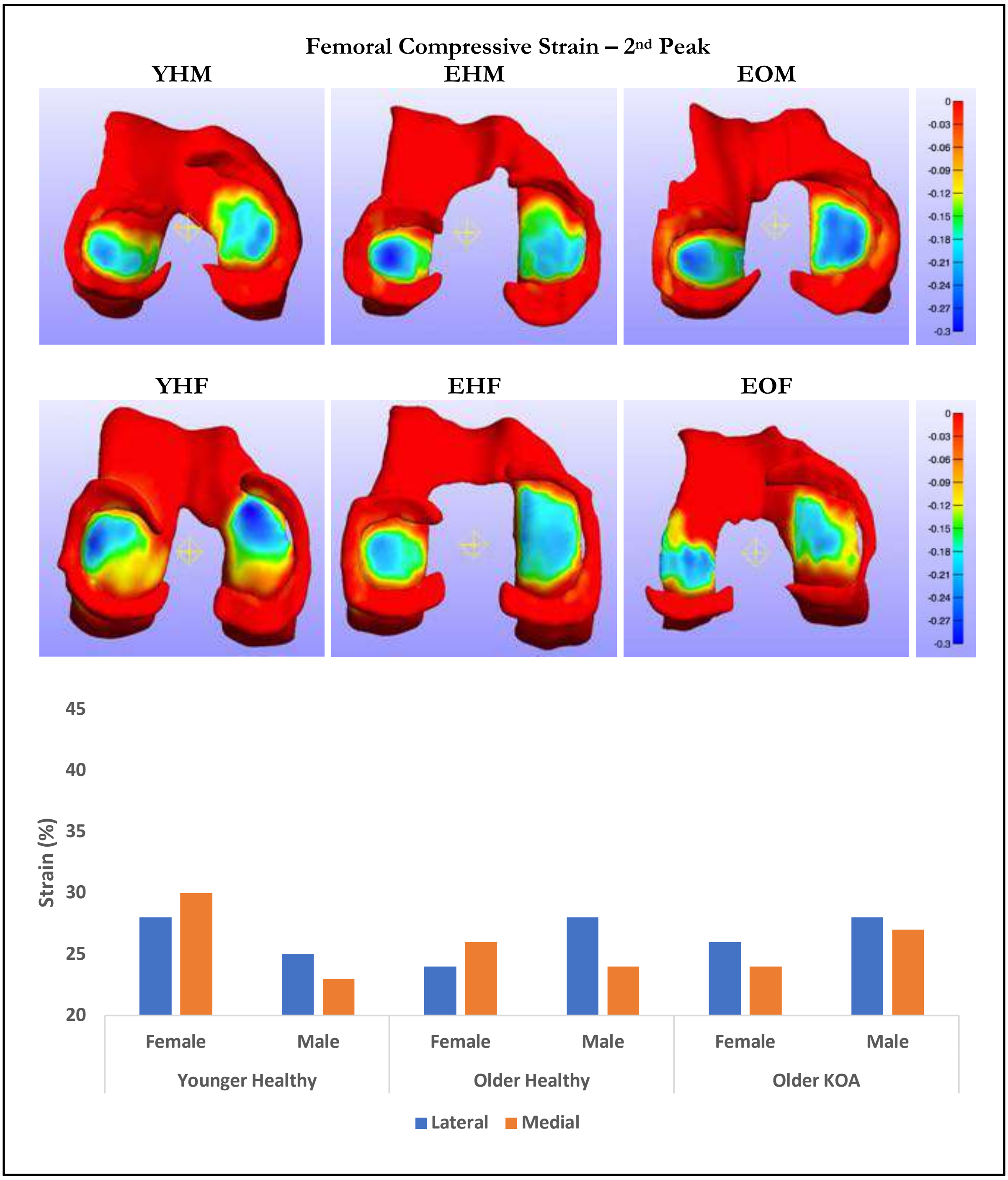

Figure 24 - Compressive strain on the femur at the 2nd peak joint contact force. Top: Visual representation of strain distribution across the cartilage surface. Bottom: Bar chart showing peak cartilage strains

5.4 Summary

This section has demonstrated the development of six subject specific finite element models of healthy and osteoarthritic subjects. Differences in stress and strain distributions in the femoral and tibial components have been found and these findings could prove important in helping us understand the pathology of mechanical pathways in early KOA. Most noteworthy were the elevated peak stresses in both compartments of the tibial cartilage experienced by elderly osteoarthritic subjects at first peak loading. Further studies are being carried out to expand the number of subjects with subject specific models so that more thorough scientific findings can be elucidated, but the work carried out here provides a clear pathway for how this can be done and is an important first step in trying to evaluate changes in cartilage mechanics in subjects with early stages of the disease. Work is also being undertaken to combine the findings from the finite element models with those found using the musculoskeletal pathways. Table 4 and Table 5 show a quantitative summary of the stresses and strains acting on the femoral and tibial cartilage at first and second peak JCF respectively

Table 4 – Femoral and tibial stresses and strains at first peak loading

	YHF	YHM	EHF	EHM	EOF	EOM
Lateral Tibia Stress (MPa)	3.45	3.67	4.45	5.57	8.13	9.1
Medial Tibia Stress (MPa)	4.38	4.11	4.57	4.01	8.55	8.9
Lateral Femur Stress (MPa)	4.01	4.77	4.8	5.74	7.5	7.7
Medial Femur Stress (MPa)	3.8	4.43	5.6	5.2	4.4	7.3
Lateral Tibia Strain (%)	23	25	26	29	33	36
Medial Tibia Strain (%)	28	24	25	23	36	42
Lateral Femur Strain (%)	25	25	22	26	31	29
Medial Femur Strain (%)	22	25	27	29	25	29

Table 5 – Femoral and tibial stresses and strains at second peak loading

	YHF	YHM	EHF	EHM	EOF	EOM
Lateral Tibia Stress (MPa)	4.35	3.71	4	4.7	9.01	6.8
Medial Tibia Stress (MPa)	6.07	3.98	3.62	4.22	7.3	7.8
Lateral Femur Stress (MPa)	5.22	4.4	4.2	5.4	6.2	5.4
Medial Femur Stress (MPa)	7.16	4.2	3.92	4.5	4.09	6.1
Lateral Tibia Strain (%)	26	23	24	29	32	35
Medial Tibia Strain (%)	32	24	23	21	30	32
Lateral Femur Strain (%)	28	25	24	28	26	28
Medial Femur Strain (%)	30	23	26	24	24	27

6 Prediction of Knee Joint Contact Forces using deep learning

6.1 Introduction

Work has been carried out to use models and techniques developed in WP3 in order to improve our understanding of joint loading in the knee through a series of projects. One of these involves investigating whether deep learning techniques can be used to predict internal forces acting on the knee without the need for complex musculoskeletal models such as those presented earlier in this report. Musculoskeletal models are robust and effective at predicting these internal forces, but they are relatively slow to run and require a lot of complex input data and extensive user experience to run efficiently. This is particularly true when trying to predict internal joint loading, where complex optimization-based techniques such as static optimization are required that are very computationally intensive. Incorporating deep learning methodologies enables joint contact forces to be predicted more quickly using only a subset of the information required by traditional musculoskeletal modelling approaches.

6.2 Methods

Subjects from the OACTIVE study were used as a training dataset for the deep learning methodologies. Knee joint kinetics and kinematic data was captured for 146 subjects and a total of 2482 individual trials, including walking and stepping trials for each leg. Data for each trial was outputted in csv format so that it could be interpreted by the computational deep learning system. Table 6 cites the characteristics (ID, name and type) of the features considered in this experimentation.

Table 6 – Characteristics of the data employed as input or output in our analysis

Feature ID	Feature name	Feature type
1	'pelvis_tilt'	Input
2	'pelvis_list'	Input
3	'pelvis_rotation'	Input
4	'pelvis_tx'	Input
5	'pelvis_ty'	Input
6	'pelvis_tz'	Input
7	'hip_flexion_l'	Input
8	'hip_adduction_l'	Input
9	'hip_rotation_l'	Input
10	'knee_angle_l'	Input
11	'knee_abd_angle_l'	Input
12	'ankle_angle_l'	Input
13	'subtalar_angle_l'	Input
14	'pelvis_tilt_moment'	Input
15	'pelvis_list_moment'	Input
16	'pelvis_rotation_moment'	Input
17	'hip_flexion_l_moment'	Input
18	'hip_adduction_l_moment'	Input
19	'hip_rotation_l_moment'	Input
20	'knee_angle_l_moment'	Input
21	'knee_abd_angle_l_moment'	Input
22	'ankle_angle_l_moment'	Input
23	'GRF_x'	Input
24	'GRF_y'	Input
25	'GRF_z'	Input
26	'KJCF_fx'	Output
27	'KJCF_fy'	Output
28	'KJCF_fz'	Output

To implement the prediction task, a multi-step ML pipeline was designed and tested. The objective of the proposed ML methodology was to estimate knee joint contact forces (variables KJCF_fx, KJCF_fy and KJCF_fz) using the rest of the features (IDs 1 to 25) as inputs (either the whole feature set of subsets of it)

The processing steps involved in the pipeline are shortly described below.

Step 1: Data pre-processing

A. Removal of features with constant values: Features that remain constant for all time steps can negatively impact the training. Thus, we found and removed the rows of data that had the same minimum and maximum values.
B. Normalization: The data predictors were normalized to have zero mean and unit variance. To calculate the mean and standard deviation over all observations, the sequence data were concatenated horizontally.
C. Data padding: To minimize the amount of padding added to the mini-batches, the training data were sorted by sequence length. Then, a mini-batch size was chosen which divides the training data evenly and reduces the amount of padding in the mini-batches.

Step 2: Data organization and data split.
Data was split into training (90%) and testing (10%) subsets. Two different approaches were adopted here:

A. 'Subject-naıve' denotes testing with models for which all trials of the test subjects were excluded from the training data.
B. 'Subject-exposed' models were trained with one or more trials of the test subjects included in the training data.

Step 3: Definition of network architecture and training
Long Short Term Memory (LSTM) networks were employed. Different network architectures were investigated for their suitability to implement the prediction task. The optimal architectures were selected for both subject-naïve and subject exposed approaches.

Step 4: Performance Validation
The performance of the proposed methodology was estimated by calculating the root mean squared error (RMSE) on the actual data ranges.

Step 5: AI explainability
Local interpretable model-agnostic explanations (LIME) were calculated to quantify the impact of the different inputs to the prediction output.

6.3 Results

A. Predictive performance of the proposed deep learning methodology

Table 7 cites the performance of the proposed LSTM-based methodology on subject-exposed data using different input feature subsets. The whole input feature set was considered in experiment 1, whereas experiments 2-4 refer to feature subsets (involving kinematics, Ground Reaction Forces and a combination of them). As it was expected, experiment 1 led to the overall best performance (RMSE of 64.8405), the second-best prediction performance was achieved in experiment 3 (RMSE of 111.1834). The worse performance was achieved by experiment 2 in which only kinematics were considered as inputs (feature IDs 1-13).

Table 7 – Results on Subject-exposed patients

exp	Input data	Network	RMSE actual			
			x	y	z	Total
1	1:25	LSTM200-FC100-FC100	28.9002	95.443	51.6544	64.8405
2	1:13	LSTM200-FC100-FC100	49.9390	272.9434	122.7483	175.1752
3	1:13 + 23:25	LSTM200-FC100-FC100	37.4680	168.1610	86.0421	111.1834
4	23:25	LSTM200-FC100-FC100	64.4981	227.7435	132.8933	156.7246

Table 8 cites the prediction performances achieved on the subject-naïve data. Here we observed a slight increase in the prediction errors. This small performance decrease was expected since the testing sets of experiments 5-8 include unseen subjects' data (all trials of the test subjects were excluded from the training data). Similarly to the results of Table 7, the best prediction accuracy in Table 8 was achieved when the full feature set was considered (experiment 5) and the second best was obtained in experiment 7 (where kinematics and GRFs are considered).

Table 8 – Results on Subject-naive patients

exp	Input data	Network	RMSE actual			
			x	y	z	Total
5	1:25	LSTM200-FC100	62.3140	152.8237	85.2180	107.2384
6	1:13	LSTM200-FC100	107.8792	470.8264	179.9574	297.6015
7	1:13 + 23:25	LSTM200-FC100	96.4757	315.4546	160.0891	211.6977
8	23:25	LSTM200-FC100	81.6902	377.7521	168.0455	243.3168

Figure 25 and Figure 26 give a visual presentation of the predicted knee joint contact forces compared to the corresponding actual values. Figure 25 shows an example on the prediction for a subject exposed data sample and Figure 26 shows an example on the prediction for a subject-naïve data sample. Overall, satisfactory prediction results are obtained for both subject-exposed and subject-naïve subjects.

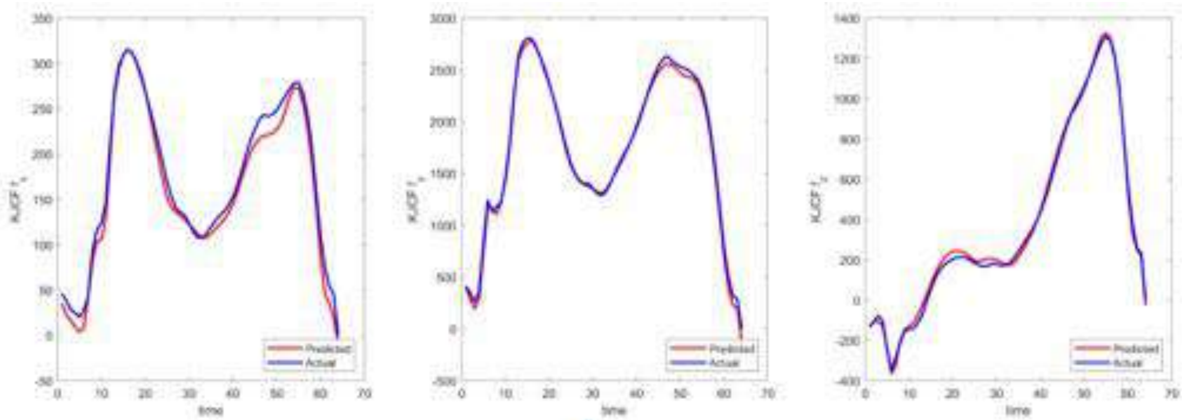

Figure 25 – Predicted (red) and actual (blue) forces on a subject-exposed patient

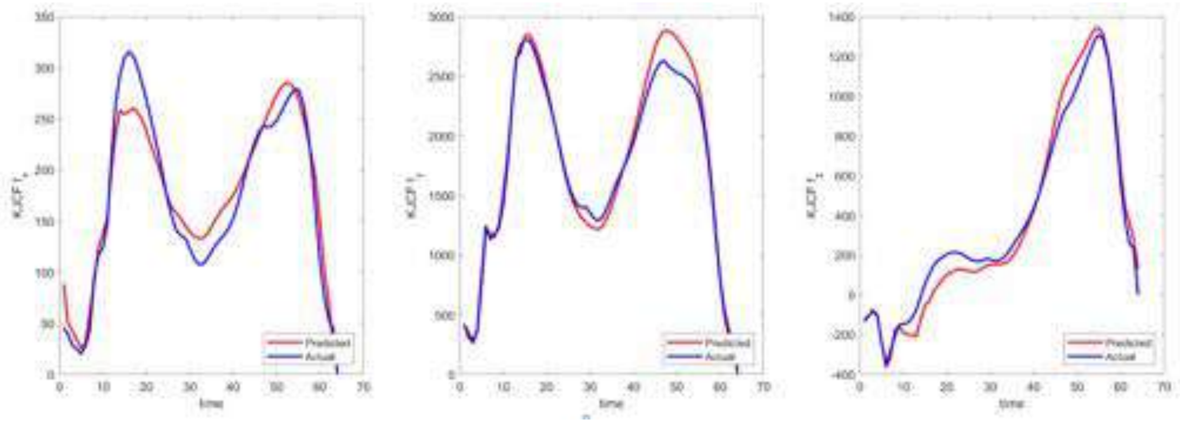

Figure 26 – Predicted (red) and actual (blue) forces on a subject-naive patient

B. *AI explainability (on exp5)*

Figure 27 below shows the significance of each feature on the decision taken by the LSTM model (in experiment 5) for a specific subject (testing). The figures show which features were activated more on the specific decision for each one of the three KJCF_F components. The explainability analysis was performed separately at each time instance and the overall effect was captured by averaging the LIME weights of all the predictions throughout the time domain of the trial.

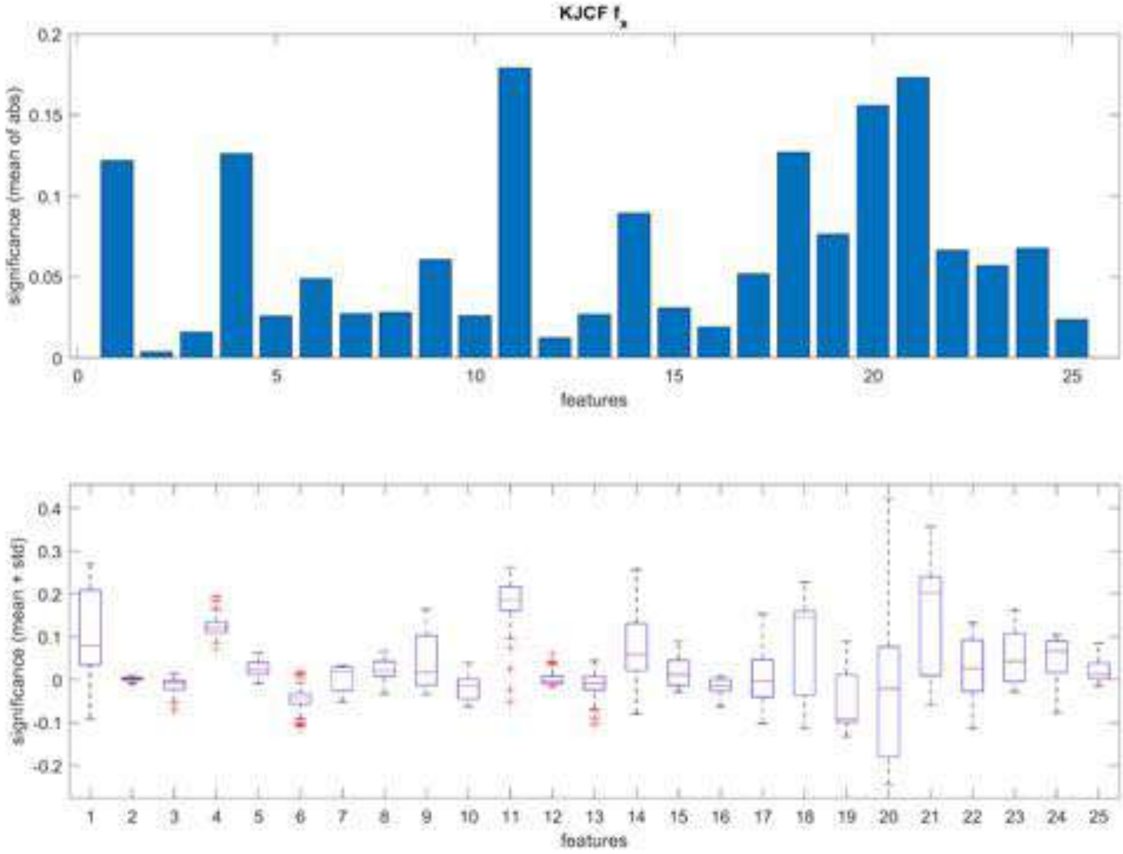
KJCF f
x
significance (mean of abs)
features
significance (mean ± std)
features

(a)

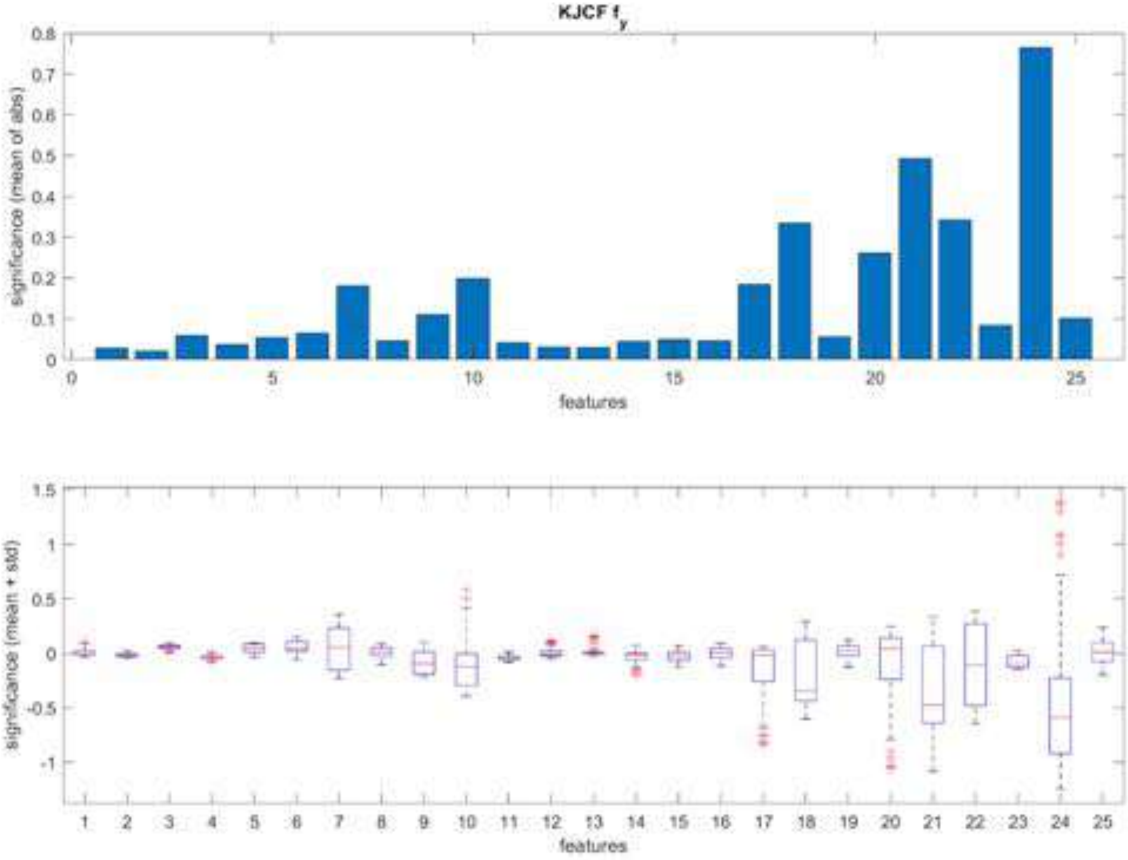
KJCF f
y
significance (mean of abs)
features
significance (mean ± std)
features

(b)

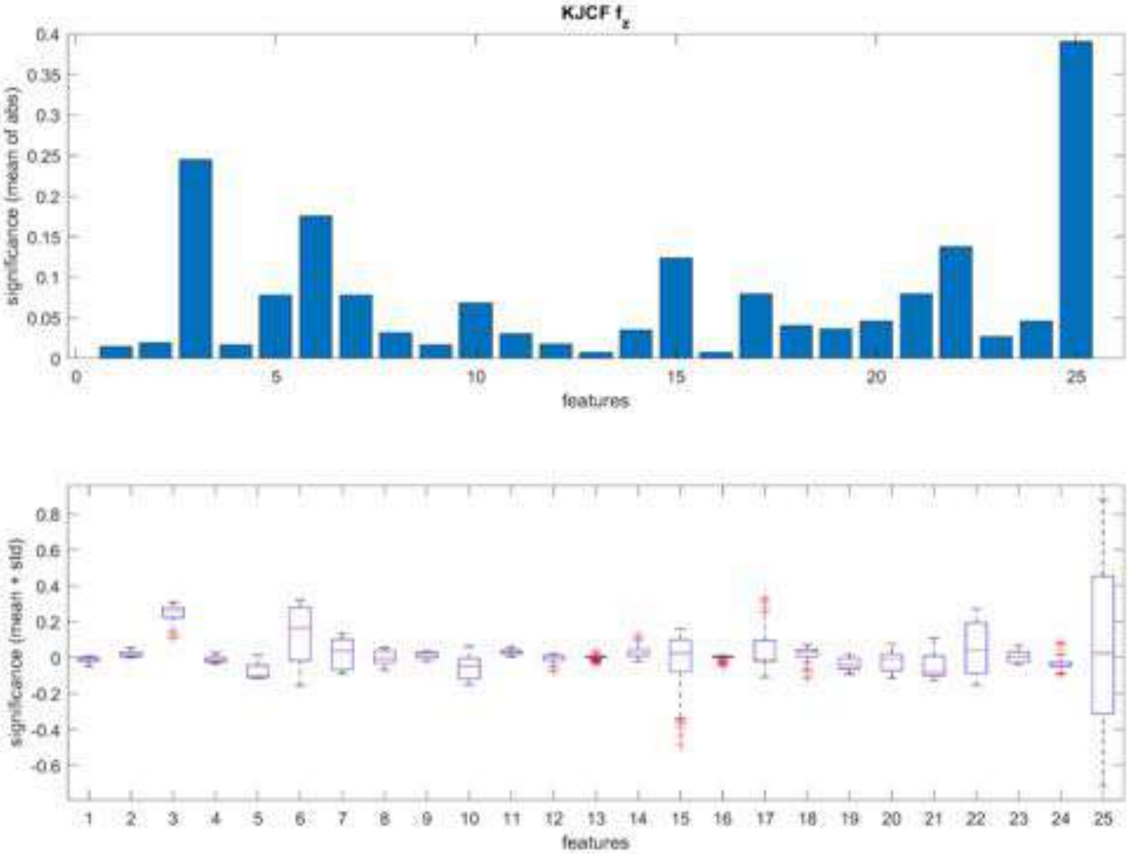

(c)

Figure 27 – Explainability results for a subject -naïve trial in which the impact of all 25 features on the prediction output is quantified for the (a) KJCF_Fx, (b) KJCF_Fy and (c) KJCF_Fz components. The top figure visualises the average significance over the whole time period of the signal, whereas the bottom figure shown the mean+std over the time period of the signal

6.4 Summary

The proposed LSTM-based methodology for the prediction of knee joint contact forces was proved to be effective as it can be seen from Figure 25 and Figure 26 and Table 7 and Table 8. In general, it was demonstrated that a deep learning modelling methodology could enable joint contact forces to be predicted more quickly using less features compared to the traditional musculoskeletal modelling approaches. Specifically, as far as the impact of selected features on the prediction accuracy, the following conclusions were extracted from the explainability analysis. (i) most important features for KJCF_Fx prediction were the following: knee_abd_angle_l, knee_abd_angle_l_moment, Knee_angle_l_moment, Pelvis_tilt, Pelvis_tx and Hip_adduction_l_moment. As far as the KJCF_Fy component, GRF_y and knee_abd_angle_l_moment had a major effect on the prediction result, whereas GRF_z and pelvis_rotation had a significant impact on the prediction of the KJCF_Fz component.

7 Investigating the correlation of cartilage stresses to KOA progression in OAI cohort

7.1 Introduction

Understanding why some subjects progress to developing KOA and some do not is important for understanding the early stages of the disease and developing early interventions. Cartilage stresses in these subjects may hold a clue as to why some subjects progress and others don't and a study is being undertaken using the methodologies and technologies developed in the OACTIVE project.

7.2 Methods

Because the subjects in the OACTIVE study itself do not have longitudinal data at the moment and so external datasets have to be used to look into the risk of progression. The OAI has a large cohort of healthy and KOA subjects, including high quality MR images suitable for segmenting and building finite element models.

Automatic MRI Segmentation

The large number of subjects in the OAI makes manual segmentation too time consuming and so automatic methods have been developed that can segment the tibial and femoral cartilage geometries automatically without the need for manual interventions. For each target image to be segmented, every atlas MRI is rigidly and affinely registered to the target to establish a spatial correspondence. After the initial registration, the best aligned atlases are chosen to provide labels for the target MRI through the application of a patch-based scheme.

The initial registration allows us to construct a pre-segmentation mask, which we use to identify the sampling area in which the subsequent step of label propagation will take place. A spatially stratified sampling method is applied to select a certain number of voxels from the target image, uniformly dispersed throughout the sampling area. Through the spatial correspondence established by the affine registration, subset voxels from the selected atlas MRIs, spatially aligned to the already sampled target voxels, are selected, along with their corresponding labels. This collection forms the initial global dataset. All voxels in the global dataset are subsequently assigned a 3D SIFT description, and a graph-based semi-supervised learning scheme is applied to propagate labels from the atlas voxels to the target voxels.

In order to assign labels to the remaining target voxels (those that were not sampled in the global dataset), the initially sampled target voxels are used to construct a 3D Delaunay tetrahedral mesh. An iterative process is initialized, whereby in each iteration, new points are inserted at the centroids of each tetrahedron. Those new points inserted at each iteration correspond to yet unlabeled target voxels, which are assigned labels through the same process of 3D SIFT encoding and semi-supervised learning. The iterative process continues until convergence, where any remaining unlabeled target voxels are assigned labels via a simple majority voting rule from their closest spatial neighbors.

After the finalization of the segmentation process, a series of post processing filters are applied to smooth the boundaries of the segmented objects. Subsequently, a surface extraction algorithm coupled with a distance transform are applied to each one of the segmented objects, resulting in an image map containing at each voxel of the corresponding segmented object, a thickness value, measuring its distance from the object surface. This thickness map is then processed to extract a geometric feature vector characterizing the thickness of the entire object.

FE Model Generation

The segmented STL files are smoothed via the processes outlined previously in this document and elsewhere in D3.1. The smoothed geometries are re-meshed to an appropriate mesh density and then outputted prior to the construction of the FE model. An artificial femoral segment is created that controls the loading and rotation of the femoral cartilage component and is attached via a rigid connection to the internal face of the femoral cartilage. The bottom faces of the tibial cartilage components are fixed in all six degrees of freedom to simulate their attachment to the tibia. The tibial cartilage components are attached to the outer face of the femoral component through a series of frictionless sliding elastic connectors. The femoral component is allowed to translate vertically and abduct/adduct into a natural position as a generic load is gradually applied up to the peak loading. This peak loading is adjusted linearly for each subject based on the subject's mass.

7.3 Results

So far only one subject has had their FE model built as a proof of concept. The results indicate that the project is highly feasible and that it is likely it will generate useful information despite the simplifications made to the model in order to facilitate higher throughput. The results from the individual subject can be seen in Figure 28.

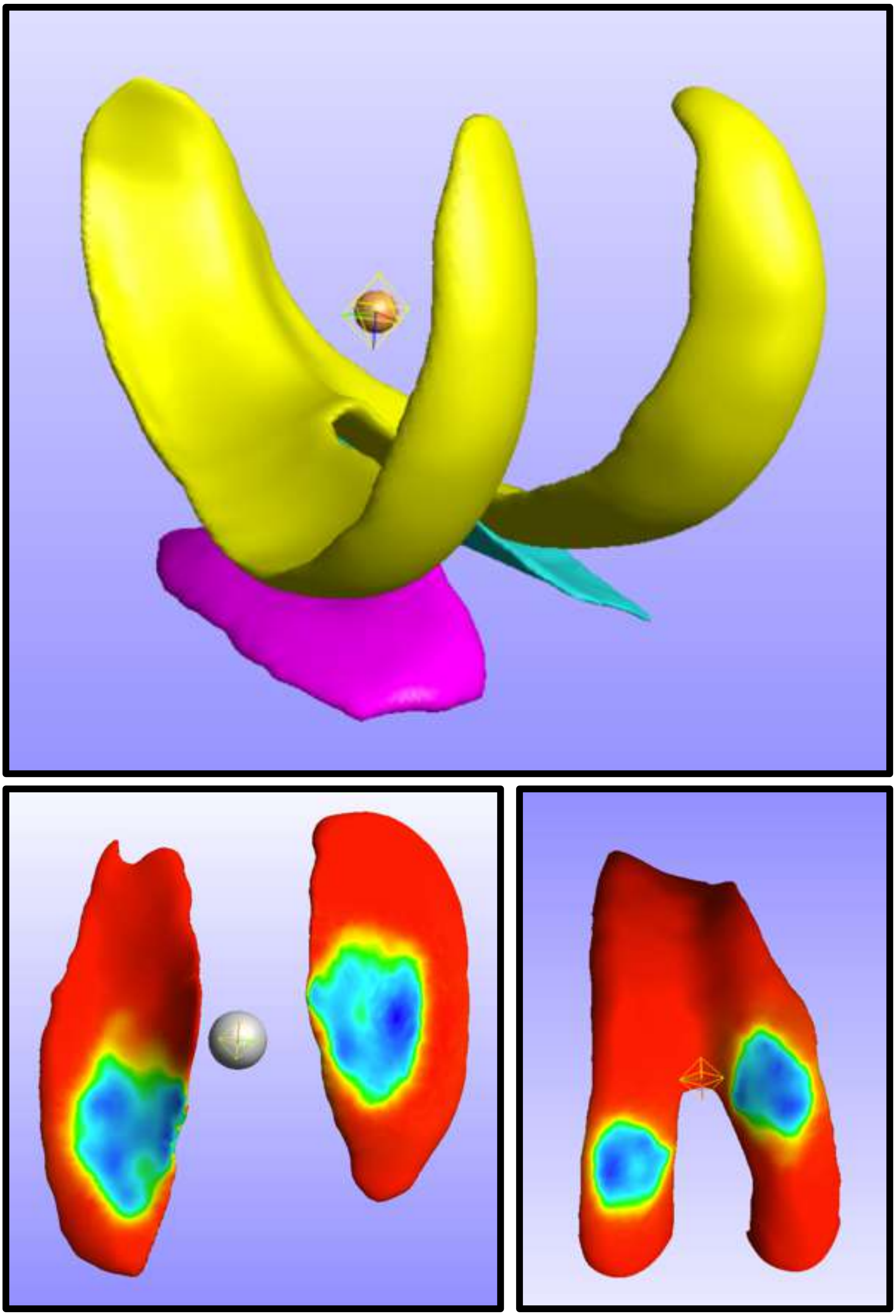

Figure 28 - Example of finite element model construction and outputs for proposed study

7.4 Summary

Results so far have highlighted the potential for technologies developed in the OACTIVE project to be applied to external datasets to generate clinical useful findings. Future work will focus on quickly generating a large number of subject specific models for OAI subjects in two groups, stratifying them into subjects that progress to KOA and those that do not. It is hoped that cartilage stress distributions in these subjects will be able to help predict KOA progression in these subjects.